Year: 2016

Semi-automated calibration method for modelling of mountain permafrost evolution in Switzerland

Marmy, Antoine ; Rajczak, Jan ; Delaloye, Reynald ; Hilbich, Christin ; Hoelzle, Martin ; Kotlarski, Sven ; Lambiel, Christophe ; Noetzli, Jeannette ; Phillips, Marcia ; Salzmann, Nadine ; Staub, Benno ; Hauck, Christian

Abstract: Permafrost is a widespread phenomenon in mountainous regions of the world such as the European Alps. Many important topics such as the future evolution of permafrost related to climate change and the detection of permafrost related to potential natural hazards sites are of major concern to our society. Numerical permafrost models are the only tools which allow for the projection of the future evolution of permafrost. Due to the complexity of the processes involved and the heterogeneity of Alpine terrain, models must be carefully calibrated, and results should be compared with observations at the site (borehole) scale. However, for large-scale applications, a site-specific model calibration for a multitude of grid points would be very time-consuming. To tackle this issue, this study presents a semi-automated calibration method using the Generalized Likelihood Uncertainty Estimation (GLUE) as implemented in a 1-D soil model (CoupModel) and applies it to six permafrost sites in the Swiss Alps. We show that this semi-automated calibration method is able to accurately reproduce the main thermal condition characteristics with some limitations at sites with unique conditions such as 3-D air or water circulation, which have to be calibrated manually. The calibration obtained was used for global and regional climate model (GCM/RCM)-based long-term climate projections un- der the A1B climate scenario (EU-ENSEMBLES project) specifically downscaled at each borehole site. The projection shows general permafrost degradation with thawing at 10 m, even partially reaching 20 m depth by the end of the century, but with different timing among the sites and with partly considerable uncertainties due to the spread of the applied climatic forcing.

DOI: https://doi.org/10.5194/tc-10-2693-2016

Originally published at:
Marmy, Antoine; Rajczak, Jan; Delaloye, Reynald; Hilbich, Christin; Hoelzle, Martin; Kotlarski, Sven; Lambiel, Christophe; Noetzli, Jeannette; Phillips, Marcia; Salzmann, Nadine; Staub, Benno; Hauck,

Christian (2016). Semi-automated calibration method for modelling of mountain permafrost evolution in Switzerland. The Cryosphere, 10(6):2693-2719.
DOI: https://doi.org/10.5194/tc-10-2693-2016

The Cryosphere, 10, 2693–2719, 2016
www.the-cryosphere.net/10/2693/2016/
doi:10.5194/tc-10-2693-2016

The Cryosphere
Open Access

Semi-automated calibration method for modelling of mountain permafrost evolution in Switzerland

Antoine Marmy[1], Jan Rajczak[2], Reynald Delaloye[1], Christin Hilbich[1], Martin Hoelzle[1], Sven Kotlarski[2], Christophe Lambiel[3], Jeannette Noetzli[4], Marcia Phillips[5], Nadine Salzmann[1], Benno Staub[1], and Christian Hauck[1]

[1]Department of Geosciences, University of Fribourg, Fribourg, Switzerland
[2]Institute for Atmospheric and Climate Science, ETH Zurich, Switzerland
[3]Institute of Earth Surface Dynamics, University of Lausanne, Lausanne, Switzerland
[4]Department of Geography. University of Zurich, Zurich, Switzerland
[5]WSL, Swiss Federal Institute for Snow and Avalanche Research, Davos, Switzerland

Correspondence to: Antoine Marmy (antoine.marmy@gmail.com)

Received: 11 July 2015 – Published in The Cryosphere Discuss.: 10 September 2015
Revised: 13 July 2016 – Accepted: 7 September 2016 – Published: 15 November 2016

Abstract. Permafrost is a widespread phenomenon in mountainous regions of the world such as the European Alps. Many important topics such as the future evolution of permafrost related to climate change and the detection of permafrost related to potential natural hazards sites are of major concern to our society. Numerical permafrost models are the only tools which allow for the projection of the future evolution of permafrost. Due to the complexity of the processes involved and the heterogeneity of Alpine terrain, models must be carefully calibrated, and results should be compared with observations at the site (borehole) scale. However, for large-scale applications, a site-specific model calibration for a multitude of grid points would be very time-consuming. To tackle this issue, this study presents a semi-automated calibration method using the Generalized Likelihood Uncertainty Estimation (GLUE) as implemented in a 1-D soil model (CoupModel) and applies it to six permafrost sites in the Swiss Alps. We show that this semi-automated calibration method is able to accurately reproduce the main thermal condition characteristics with some limitations at sites with unique conditions such as 3-D air or water circulation, which have to be calibrated manually. The calibration obtained was used for global and regional climate model (GCM/RCM)-based long-term climate projections under the A1B climate scenario (EU-ENSEMBLES project) specifically downscaled at each borehole site. The projection shows general permafrost degradation with thawing at 10 m, even partially reaching 20 m depth by the end of the century, but with different timing among the sites and with partly considerable uncertainties due to the spread of the applied climatic forcing.

1 Introduction

Permafrost is the thermal state of a soil or rock subsurface with a temperature that remains below 0 °C for two or more consecutive years (Harris et al., 2009). It occurs in the Arctic (Romanovsky et al., 2010) and Antarctic ice-free regions (Vieira et al., 2010) as well as in mid-latitude mountain ranges such as in the European Alps (Boeckli et al., 2012), the Andes (Trombotto, 2000) and the Himalayan range (Weiming et al., 2012). In the last few decades, in the context of global warming, interest in permafrost has increased for various reasons such as greenhouse gas release (e.g. Anthony et al., 2012), engineering and construction issues (e.g. Lepage and Doré, 2010; Bommer et al., 2010), water management issues (e.g. Quinton et al., 2011) and slope stability concerns (McColl, 2012). In mountain environments, the increase in air temperatures observed in the last decades (Mountain Research Initiative EDW Working Group, 2015) has had notable effects on permafrost that are apparent: (i) in the borehole data series by higher surface and subsurface ground temperatures and significantly deeper active layers (e.g. PERMOS, 2016), (ii) in geophysical data with a decrease of the electrical resistivities (Hilbich

Published by Copernicus Publications on behalf of the European Geosciences Union.

et al., 2008, 2011; PERMOS, 2016) and of seismic velocities (Hilbich, 2010), indicating a reduction of ice content, and (iii) in the increased activity of permafrost creep (Kääb and Kneisel, 2006; Barboux et al., 2013) and increased velocities of instable rock glaciers (Kääb et al., 2007; Gärtner-Roer, 2012).

Therefore, increasing effort has recently been put into permafrost modelling across different temporal and spatial scales. The conceptual and spatial range of modelling approaches include (i) physically based process and/or energy balance models, which focus either on 3-D applications by simulating a limited number of processes such as heat conduction, latent heat and the effect of topography (e.g. Noetzli and Gruber, 2009; Noetzli et al., 2007) or on 1-D simulations to analyse a large number of complex subsurface processes with a potentially high number of feedback mechanisms (e.g. Westermann et al., 2015, 2016; Langer et al., 2013; Hipp et al., 2012; Scherler et al., 2010; Luetschg et al., 2008), and (ii) empirical–statistical distribution models (e.g. Etzelmüller et al., 2006; Hartikainen et al., 2010; Boeckli et al., 2012; Sattler et al., 2016), which are often based on rock glacier inventories or other permafrost evidence (Cremonese et al., 2011). Recently, new model approaches have been developed that are able to simulate hydrological processes in 3-D, while keeping most thermal processes in 1-D (Endrizzi et al., 2014). On hemispheric and global scales, spatially distributed 1-D models (also called 2.5-D models) and land surface schemes are used to assess permafrost evolution. Here, ground temperatures are only calculated along 1-D soil columns, but on a large regional or hemispheric grid (e.g. Jafarov et al., 2012; Zhang et al., 2012; Westermann et al., 2013, 2016; Ekici et al., 2014, 2015; Chadburn et al., 2015) without lateral interaction.

The 3-D and 2-D approaches can be related more easily to geophysical or remote sensing methods, especially in Arctic lowlands where methane release is a major issue (Anisimov, 2007). In mountain environments, 1-D modelling is widely used due to the spatial heterogeneity of surface and subsurface composition, topography, morphological landforms and microclimatic processes. Moreover, 1-D approaches are easier to relate to borehole temperature time series that are common in Alpine permafrost research and are usually the only validation or calibration data available. However, the final goal of most permafrost modelling studies, especially in the Arctic (e.g. Ekici et al., 2015), is the representation of permafrost and permafrost processes in a distributed model. Whereas this is common in the Arctic, this is still at a beginning stage in Alpine environments due to many limiting factors, including the scarcity of input data and the heterogeneity of surface, subsurface and microclimatical conditions. Fiddes et al. (2015) proposed a scheme that is leading in the direction of combining physically based land surface models and gridded climate data to efficiently simulate air temperature and near-surface ground temperature, but it does not include borehole data validation.

Site-specific calibration is an important prerequisite for successful permafrost modelling with complex models. However the process of calibration often faces the scarcity of measured input parameters such as porosity, ice and water content or thermal and hydraulic conductivities. All modelling approaches trying to simulate real conditions should use a specific procedure (Westermann et al., 2013), which can also include empirical calibration methods by manual tuning (Gruber and Hoelzle, 2001; Hipp et al., 2012; Scherler et al., 2013). With recent improvements in computing capacity, the use of automated procedures of inverse modelling approaches using Monte Carlo chains has become increasingly attractive (Jansson, 2012; Heerema et al., 2013), but so far this approach has not been tested in permafrost research.

The final goal of most permafrost modelling studies is their application to long-term climate impact simulations. Previous studies of combined climate–permafrost simulations with explicit subsurface simulations for the Alps are rare and were focused only on one or two sites (e.g. Engelhardt et al., 2010; Scherler et al., 2013) because of the limitations in the availability of ground temperature data and/or onsite meteorological data for calibration/validation purposes. Atmospheric forcing data for permafrost models can be derived from global and/or regional climate models (GCMs, RCMs). Especially for Alpine terrain, RCMs offer an added value with respect to coarse-resolution GCMs (e.g. Kendon et al., 2010; Torma et al., 2015), and are now widely used in scientific research, especially in the impact modelling community (e.g. Bosshard et al., 2014).

In this study, we present a semi-automated procedure for calibrating a soil model to a large number of points at multiple permafrost sites. The calibration procedure attempts to understand site-specific differences as well as to quantify the sensitivity of the soil model to the tested parameters. The procedure has been applied to six test sites in the Swiss Alps: Stockhorn, Schilthorn, Muot da Barba Peider, Lapires, Murtèl-Corvatsch and Ritigraben. After calibration, the model set-up was used for long-term simulations driven by downscaled climate model data until the end of the 21st century, and an analysis of the evolution of the ground thermal regime and the snow cover is presented. The present work has two main objectives: (i) to show the benefits and limitations of a semi-automated calibration procedure for detailed soil process modelling in permafrost terrain, using this procedure to identify differences and similarities among the test sites and to assess the sensitivity of the soil model to certain parameters, and (ii) to develop scenarios of the possible evolution of mountain permafrost in Switzerland.

2 Study sites

In the framework of the SNF-funded project "The Evolution of Mountain Permafrost of Switzerland" (TEMPS) (Hauck et al., 2013) and the Swiss permafrost monitoring network PERMOS (PERMOS, 2016), based on the collaboration of five research institutions, the data sets necessary for calibration and validation purposes were available for six different sites in the Swiss Alps (PERMOS data, 2016). These sites cover a broad geographical range within Switzerland and represent a variety of landforms including rock slopes/plateaus, talus slopes and rock glaciers. The choice of the following sites was mainly driven by the availability of long-term time series of borehole temperatures and meteorological observations.

2.1 Schilthorn

The Schilthorn massif site (SCH) is situated at 2970 m a.s.l. (above sea level) in the north-central part of the Swiss Alps. The lithology of this non-vegetated site is dominated by deeply weathered dark limestone schists forming a surface layer of mainly sandy and gravelly debris up to several metres in thickness over presumably strongly jointed bedrock. Within the framework of the European PACE project (Harris et al., 2003), the site was chosen for long-term permafrost observation and was consequently integrated into the Swiss permafrost monitoring network PERMOS as one of its reference sites (PERMOS, 2016). The monitoring station at 2910 m a.s.l. is located on a small plateau on the north-facing slope, and comprises a meteorological station (shortwave and long-wave radiation, air temperature, humidity, snow height, wind speed and direction) and three boreholes (14 m vertical, 100 m vertical and 100 m inclined) with continuous ground temperature measurements from 1999 onwards (Vonder Mühll et al., 2000; Hoelzle and Gruber, 2008; Noetzli et al., 2008; Harris et al., 2009; PERMOS, 2016). Borehole data indicate permafrost of at least 100 m thickness, which is characterized by ice-poor conditions close to the melting point. Maximum active-layer depths recorded since the start of measurements in 1999 were generally around 4–5 m until the year 2008 but have increased to 6–7 m since 2009. During the superposition of the very warm winter of 2002/2003 with the summer heatwave of 2003 (Schär et al., 2004), the active-layer depth increased exceptionally to 8.6 m, reflecting the potential for degradation of permafrost at this site (Hilbich et al., 2008).

The monitoring station is complemented by soil moisture measurements from 2007 onwards and geophysical (mainly geoelectrical) monitoring from 1999 onwards (Hauck, 2002; Hilbich et al., 2011; Pellet et al., 2016). The snow cover at Schilthorn can reach maximum depths of about 2–3 m and usually lasts from October through to June/July.

2.2 Murtèl-Corvatsch rock glacier

The rock glacier Murtèl-Corvatsch (COR) is situated in the Upper Engadine, eastern Swiss Alps, and ranges from 2750 to 2600 m a.s.l., facing north–northwest. The surface consists of large blocks of up to several metres high, which are composed of granodiorite and metamorphosed basalt (Schneider et al., 2013). Below this coarse blocky surface layer of approximately 3–3.5 m in thickness, a massive ice core (up to 90 %, Haeberli, 1990; Haeberli et al., 1998; Vonder Mühll and Haeberli, 1990) is present down to 28 m, with a frozen blocky layer below reaching from 28 to 50 m, probably adjacent to the bedrock (Arenson et al., 2002).

The main monitoring station is situated on a flat ridge at 2670 m a.s.l. and comprises a meteorological station (short- and long-wave radiation, air temperature, surface temperature, humidity, snow height, wind speed and direction) established in 1997 (Mittaz et al., 2000; Hoelzle et al., 2002; Hoelzle and Gruber, 2008) and two boreholes drilled in 1987 and 2000 (PERMOS, 2016), which show significant small-scale heterogeneities in the rock glacier (Vonder Mühll et al., 2001; Arenson et al., 2010). Permafrost temperatures are around −2 °C at 10 m depth, and the active layer has a thickness of 3.2 m on average. Annual precipitation at the site is about 900 mm (982 mm St Moritz 1951–1980; 856 mm Piz Corvatsch 1984–1997), with a typical snow cover thickness of 1–2 m. Mean annual air temperature (MAAT) is −1.7 °C for the observation period of March 1997 to March 2008 (Scherler et al., 2014). Geophysical monitoring (mainly ERT) has been conducted since 2005 (Hilbich et al., 2009).

2.3 Lapires

The Lapires (LAP) talus slope is located on the western slope of Val de Nendaz in Valais (46°06′ N, 7°17′ E) in the western Swiss Alps, ranging from 2350 to 2700 m a.s.l. with a north–northeast orientation. Its surface consists of gneiss schists, and the talus shows a thickness of more than 40 m at the locations of the boreholes described below. Snow avalanches and minor rockfalls with variable frequencies from one year to another affect the slope (Delaloye, 2004; Delaloye and Lambiel, 2005; Lambiel, 2006). The Lapires talus slope shows an active layer of about 4–5.5 m thickness situated on top of an ice-rich (30–60 %) permafrost layer of around 15 m thickness, with temperatures very close to the melting point (Scapozza et al., 2015; Staub et al., 2015).

The monitoring station consists of a meteorological station (air temperature and shortwave radiation since 1998, wind speed and direction and snow depths since 2009) installed in 1998 and three further boreholes installed in 2008 along a longitudinal profile (Scapozza et al., 2015). MAAT was +0.5 °C at 2500 m a.s.l.

Compared to the strong microtopography of Murtèl rock glacier, the Lapires talus slope is comparatively homogeneous regarding slope and microtopography. The permafrost distribution within the talus slope is discontinuous (mainly related to heterogeneous substrate dominated by fine-grained material in the western part and coarse-blocky material in the eastern part) and linked to a complex system of internal air circulation, also called the “chimney effect” (Delaloye and Lambiel, 2005). This air circulation is responsible for ground cooling at the bottom of the talus slope, where cold air is sucked up in winter. These 2-D (or potentially 3-D) processes cannot be explicitly simulated by the CoupModel; however, their effect on the thermal regime has been indirectly confirmed by specific 1-D distributed CoupModel simulations at this site (Staub et al., 2015).

2.4 Ritigraben

The active rock glacier Ritigraben (RIT) is located in the area Grächen-Seetalhorn (46°11′ N, 7°51′ E), Valais, western Swiss Alps, and covers an area between elevations of 2260 m and 2800 m a.s.l. Block sizes at the surface range from 0.5 up to several cubic metres. Active layer depth is almost constant at 4 m.

A 30 m borehole was drilled in 2002 in the lower part of the rock glacier at an altitude of 2615 m a.s.l., which is gradually being sheared off from the base upwards due to the movement of the rock glacier. As a result, temperature is currently only measured to a depth of 13 m. Borehole temperatures indicate the formation of a seasonal talik between 11 and 13 m depth, which appears to be directly linked to snow meltwater and rainfall infiltration (Zenklusen Mutter and Phillips, 2012). The effect of these processes on the thermal regime has recently been analysed by explicit process modelling using the model SNOWPACK (Luethi et al., 2016).

The monitoring station is complemented by an automated weather station (net radiation, air temperature and relative humidity, surface temperature, snow depth, precipitation and wind speed and direction) installed in 2002 (Herz et al., 2003).

2.5 Muot da Barba Peider

The Muot da Barba Peider (MBP) talus slope is located near the top of the NW-oriented flank of the Muot da Barba Peider ridge at 2960 m a.s.l. above the village of Pontresina, Upper Engadine, eastern Swiss Alps. The slope is 38° steep and is covered with coarse blocks (Zenklusen Mutter et al., 2010). The bedrock consists of gneiss from the upper Austroalpine nappe. Two adjacent (50 m apart) 18 m deep boreholes were drilled in 1996.

The drilling stratigraphy shows ground ice occurrences inside the talus, which reach a depth of about 4 m, with frozen bedrock below (Rist et al., 2006). Active layer depth varies between 1 and 2 m (Zenklusen Mutter et al., 2010). Due to the presence of experimental snow avalanche defence structures near borehole 1, the snow cover persists longer there in spring/summer, and thus influences the ground thermal regime (Phillips, 2006).

An automatic weather station was installed in 2003, showing MAAT of −3 °C. Regional values for mean annual precipitation are around 1500 mm at this elevation (Zenklusen Mutter and Phillips, 2012). Maximum snow depths have ranged between 0.5 and 3 m since 2003.

2.6 Stockhorn

The study site of the Stockhorn (STO) plateau is situated on an east–west-oriented mountain crest around 3410 m a.s.l., to the west of the Stockhorn summit (3532 m a.s.l.) above Zermatt (45°59′ N, 7°49′ E), western Swiss Alps. The lithology consists of Albit-Muskowit schists, and the surface is characterized by patterned ground that has developed in a thin debris cover. Significant amounts of ground ice could be observed in large ice-filled cracks during construction works of a new ski lift in summer 2007 (Hilbich, 2009). Two boreholes only 30 m apart were drilled in 2000 as part of the PACE project (Harris et al., 2003). The recorded borehole temperatures show that the Stockhorn plateau is strongly affected by 3-D topography effects (Gruber et al., 2004) because the 100 m deep borehole close to the north face exhibits significantly colder temperatures than the borehole 17 m deep located close to the southern edge of the plateau. A meteorological station (measuring shortwave and long-wave radiation, air temperature, humidity, snow height, wind speed and direction) was installed in 2002. A soil moisture station was added in 2014.

The MAAT at this site is −6.4 °C for 2002–2012, and the annual precipitation is around 1500 mm (Gruber et al., 2004; based on King, 1990, and Begert et al., 2003). This site is characterized by low precipitation and high solar radiation (mean shortwave incoming radiation from 2002 to 2013: 209.3 W m^{-2}) due to particular conditions created by surrounding mountain ranges exceeding 4000 m a.s.l. (Gruber et al., 2004).

3 Data and model

One of the main challenges in the modelling of permafrost evolution is the general lack of long (> 15 years) and complete on-site meteorological data necessary as input for the calibration of the soil model. Similarly, data from GCM/RCM-derived climate scenarios have to be downscaled and bias-corrected to obtain specific on-site conditions, which is non-trivial due to the high altitudes of most permafrost stations and the above-mentioned short length of on-site meteorological data. In this section we will explain the downscaling and bias correction approach used, and introduce the available borehole data sets used for calibration of the soil model. Finally, the physical basis of this so-called CoupModel as well as its major parameterizations will be explained.

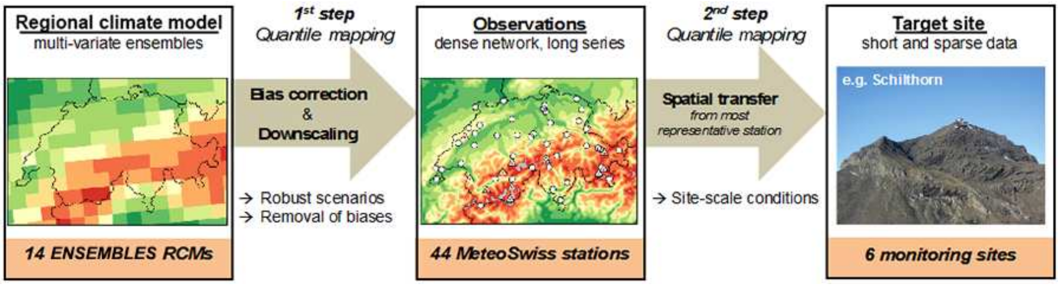

Figure 1. Schematics of the two-step procedure used for the generation of climate scenarios at the six monitoring sites. Figure adapted from Rajczak et al. (2016).

3.1 Climate scenarios: statistical downscaling and bias correction

Site-specific climate scenarios have been developed for eight meteorological variables at daily resolution for the period from 1951 to 2099 (Rajczak et al., 2016). The scenarios are based on an ensemble of 14 regional climate model (RCM) projections from the EU ENSEMBLES project (van der Linden and Mitchell, 2009). It should be noted that some variables have fewer GCM/RCM chains available: 7 for mean wind speed and maximum wind gusts and 13 for global radiation. Only the 13 chains with global radiation were used in the present study.

The ensemble accounts for a comprehensive range of model uncertainty, and is forced by the IPCC SRES A1B emission scenario (Nakicenovic and Swart, 2000). Due to their limited spatial resolution, site-specific features are typically not resolved by climate models, and even on resolved scales, models are subject to biases (e.g. Kotlarski et al., 2014). Statistical downscaling (SD) and bias correction (BC) techniques serve to attain representative conditions for the site scale and to remove model biases. SD/BC applications derive an empirical relationship between observations and model output. The established relationships are in turn used to translate long-term climate simulations to the site scale. Calibrating SD/BC techniques, however, requires long-term observations (e.g. 30 years and more), a prerequisite not met by the monitoring sites of the present study.

To obtain robust and reliable climate scenarios at the six considered sites, a newly implemented SD/BC method was used that specifically targets locations that lack long-term data. A detailed description and comprehensive validation of the approach is given by Rajczak et al. (2016). It is designed as a two-step procedure sketched in Fig. 1. In the first step, climate model simulations are downscaled to match long-term observational measurements at a most representative site (MRS) within a surrounding measurement network (e.g. MeteoSwiss weather stations). In the second step, the downscaled and bias-corrected time series from the MRS are spatially transferred to the site of interest (e.g. a permafrost monitoring site). Both steps rely on the quantile mapping (QM) method, a well-established statistical downscaling and bias correction technique (e.g. Themessl et al., 2011). The concept behind QM is to correct the distribution of a given predictor (e.g. climate model output) in such a way that it matches the distribution of a predictand (e.g. observations of the same variable at a monitoring site). Values outside the range of calibrated values are treated using the correction for the 1st (99th) quantile. Within this study, the spatial transfer is performed from an objectively selected MRS within the MeteoSwiss monitoring network. Consequently, Rajczak et al. (2016) show that the MRS is, in many cases, not the closest station but rather one at a similar altitude.

3.1.1 Reconstruction of meteorological observations

The two-step procedure (Fig. 1) additionally facilitates the reconstruction of data at the monitoring sites for non-measured periods. The concept behind reconstructing data is to spatially transfer (Fig. 1, step 2) observed values from an MRS to the target site. In the framework of the present study, data were reconstructed for some periods between 1981 and 2013. Note, that reconstruction is constrained by the availability of data at the MRS. An extensive validation of the reconstruction performance is given by Rajczak et al. (2016).

3.1.2 Climate scenarios: projections of 2 m temperature

Based on the developed site-scale scenarios, Fig. 2 provides the projected evolution of mean annual air temperature (MAAT) at 2 m above ground for the six considered sites in the period between 1961 and 2099. The projections assume an A1B emission scenario and include model uncertainty (i.e. range of estimates). While MAAT is predominantly negative in present-day climate, all six sites are subject to a significant increase in temperature and the majority of climate models indicate positive mean annual temperatures by the end of the 21st century at four of the six sites.

For each site, the reconstructed meteorological data consist of daily series for the period between 1981 and 2013 for five variables: mean air temperature, precipitation sum, mean wind speed, mean relative humidity and global radia-

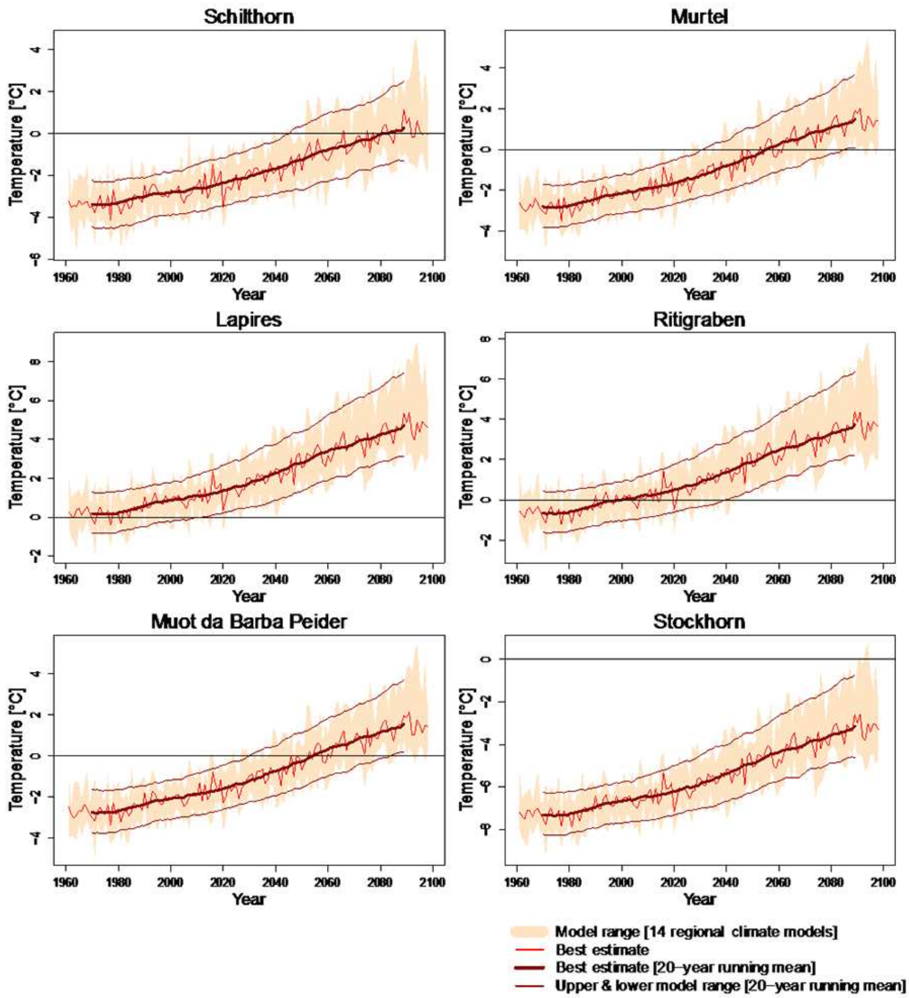

Figure 2. Site-scale climate scenarios of mean annual air temperature at 2 m above ground (MAAT) for the six considered permafrost monitoring sites. The results are based on the developed scenarios using the two-step procedure (Fig. 1) and are based on 14 ENSEMBLES regional climate models assuming an A1B greenhouse gas emission scenario.

tion. For the site MBP, the global radiation series could not be reconstructed because of a lack of validation data and could therefore not be used as forcing variable in the calibration for this site. Global radiation for MBP has therefore been estimated by CoupModel based on potential global radiation (depending on latitude and declination) and atmospheric turbidity (Jansson, 2012). Independent comparison between measured, reconstructed and CoupModel-estimated global radiation values for COR showed an overestimation of global radiation by the CoupModel leading to near-surface maximum temperature biases of up to 10 °C in summer (cf. Supplement). However, the calibration technique applied (see Sects. 4 and 5) would compensate potential biases in the temperature simulations by adjusting related parameters in the model, e.g. snow cover parameters or the albedo. Corresponding uncertainties arising from a potential compensation in the MBP results will be further discussed below.

Despite the good quality of the reconstruction, some short gaps could not be avoided. These gaps have been filled by artificial random selection of data from other years at the same date. This method is satisfactory as the gaps are short and infrequent.

For seven of the chains, wind speed scenarios were not available. As the wind speed scenarios of all available GCM-RCM chains are very similar, we consider it acceptable to use the median of these scenarios as a substitute for the seven chains with missing wind speed scenarios.

3.2 Borehole data

For calibration, we used series of borehole temperature data for each site with a minimum length of 10 years (Table 1). Borehole data are often considered as “ground truth data”, but potential measurement errors are possible due to several reasons (such as sensor or logger drift, logger failure and in-

Table 1. Maximal depth, number of temperature sensors and series length of the boreholes used for calibration.

	Maximal depth (m)	Number of sensors	Series length
COR	57.95	53	Jul 1987–Feb 2013
LAP	19.6	19	Oct 1999–Dec 2012
MBP	17.5	10	Oct 1996–Jun 2011
RIT	25	10	Mar 2002–Sep 2012
SCH	13.7	17	Nov 1998–Jul 2013
STO	98.3	25	Oct 2002–Jun 2013

filtration of water inside the borehole casing, to name a few). Borehole data in mountainous terrain are also influenced by 3-D thermal and hydrological processes (cf. Gruber et al., 2004; Lüthi et al., 2016), which are a source of additional uncertainty in 1-D model studies, especially in areas with large topographic variability. Further, an unequal repartition of data gaps may introduce a bias in the calibration. The gaps within the borehole temperature series have not been filled in order to avoid the introduction of inconsistency and additional errors in the data used for calibration. Periods with gaps are consequently ignored in the calibration process.

3.3 CoupModel description and experimental set-up

The model used for this study is the CoupModel, a 1-D numerical model combining soil, snow and atmospheric processes (Jansson and Karlberg, 2004; Jansson, 2012). This model has already shown that it is well suited to simulate mountain permafrost processes at Schilthorn (Engelhardt et al., 2010, Scherler et al., 2010, 2013; Marmy et al., 2013) and Murtèl rock glacier (Scherler et al., 2013, 2014). It also includes an optional procedure for semi-automatic calibration based on statistical indicators (see Sect. 4).

The model couples the water and heat transfer of the soil using the general heat flow equation:

$$\frac{\delta(CT)}{\delta t} - L_{\mathrm{f}}\rho\frac{\delta\Theta_{\mathrm{i}}}{\delta t} = \frac{\delta}{\delta z}\left(k\frac{\delta T}{\mathrm{d}z}\right) - C_{\mathrm{w}}T\frac{\delta q_{\mathrm{w}}}{\delta z} - L_{\mathrm{v}}\frac{\delta q_{\mathrm{v}}}{\delta z}, \quad (1)$$

where C (J K^{-1}) is the heat capacity of soil, C_{w} (J K^{-1}) is the heat capacity of water, $T(z, t)$ (K) is the soil temperature, L_{f} and L_{v} (J kg^{-1}) are the latent heat of freezing and vapour, ρ (kg m^{-3}) is the density, $\Theta_{\mathrm{i}}(z, t)$ is the volumetric ice content, k (W m^{-1} K^{-1}) is the thermal conductivity, t is the time, z is the depth and $q_{\mathrm{w}}(z, t)$ and $q_{\mathrm{v}}(z, t)$ (kg m^{-2} s^{-1}) are the water and vapour fluxes.

The lower boundary condition is derived from the sine variation of the temperature at the soil surface and a damping factor with depth. The maximum model depth is different for the various sites due to the varying maximum depth of the available boreholes, but it is at least 30 m for all sites and well below the depth of zero annual amplitude (see Fig. 3). The prescribed heat flux at the lower boundary condition is therefore negligible. This enables comparatively stable conditions at the lower boundary, and accounts for the often isothermal conditions found in Alpine permafrost at this depth (Scherler et al., 2013; PERMOS, 2016). However, the long-term variability of permafrost conditions at the lower boundary cannot be simulated using this approach. The hydraulic boundary condition is given by gravity-driven percolation if the lowest compartment is unsaturated.

The upper boundary condition is calculated using the complete energy balance at the soil surface (or snow surface, if present). The convective heat inflow of water is given by precipitation and snowmelt multiplied by the surface temperature and the heat capacity of liquid water (C_{w}):

$$q_{\mathrm{h}}(0) = \frac{T_{\mathrm{s}} - T_1}{\Delta_z/2} + C_{\mathrm{w}}\left(T_{\mathrm{a}} - \Delta T_{\mathrm{Pa}}\right) q_{\mathrm{w}}(0) + L_{\mathrm{v}} q_{\mathrm{v}}(0) \quad (2)$$

where $q_{\mathrm{h}}(0)$ (J m^{-2} day^{-1}) is the soil surface heat flow, T_{s} is the soil surface temperature, T_1 is the temperature in the uppermost soil layer, ΔT_{Pa} is a parameter representing the temperature difference between air and precipitation, $q_{\mathrm{v}}(0)$ and $q_{\mathrm{w}}(0)$ are the vapour and water fluxes at the surface and L_{v} is the latent heat of vapour. For periods with snow cover, the upper boundary condition is calculated assuming a steady-state heat flow between the soil and a homogeneous snowpack using the thermal conductivity of snow. Temporally changing insulation conditions of the snow cover can be simulated by a critical snow height that corresponds to the snow height that completely covers the soil. It mainly depends on the surface roughness and reflects the fact that 50 cm of snow induces different insulation properties for a surface consisting of 1–2 m high boulders (e.g. for a rock glacier, COR) compared to a rather homogenous surface covered by sandy soil (e.g. at SCH; cf. also the discussion in Staub and Delaloye, 2016). The fraction of bare soil is then calculated by a ratio between 0 and this threshold (see Table 2) and further used to estimate the average soil surface temperature and surface albedo. This critical snow height is one of the parameters with the largest influence in our calibration procedure.

Snow is simulated by partitioning precipitation into rain and snow depending on temperature threshold parameters. The snow cover is assumed to be horizontally and vertically homogenous. Snowmelt is estimated as part of the heat balance of the snowpack, including net radiation, sensible and latent heat flux to the atmosphere, heat flux in precipitation, snow temperature change and heat flux to the soil. Further important processes in CoupModel are listed in Table 2 together with the respective equations. Symbols and units are listed in Appendix A.

The soil structure consists of 18 to 25 compartments (depending on the site) with increasing thickness with depth, ranging from 0.1 m in the upper layers to 4 m in the lower layers (Fig. 3). Initial conditions are estimated by the model using the first values of the meteorological data series. To avoid imprecise initial conditions, the model is run from

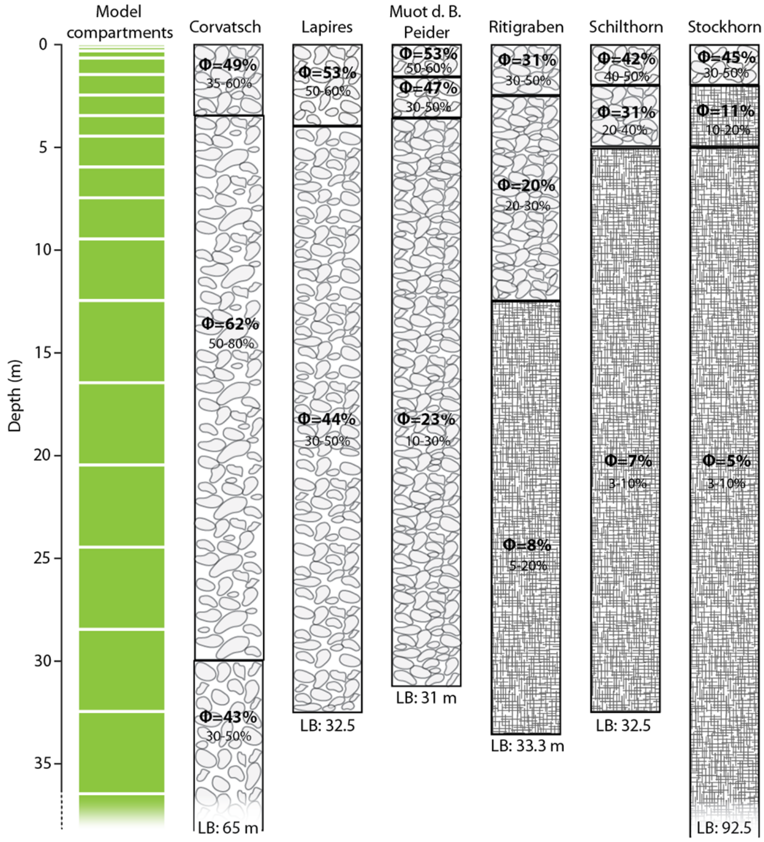

Figure 3. Description of the model layers as defined in the model (green) and of the simulated subsurface structure for each site. The depths of the horizons were estimated by experts, based on data from boreholes and geophysical surveys, whereas the porosity Φ is defined by the GLUE calibration based on the ranges estimated by the experts (given below the GLUE estimated porosity values). The maximum depth for each site (lower boundary, LB) is given below each column.

1981 onwards, although observational time series usually begin around the year 2000. No additional spin up is needed as the model usually reaches stable conditions (i.e. not influenced by initial conditions) after 10 to 15 years. Model tests with longer spin-up times only showed negligible differences with respect to the procedure described above, which may also be due to low ice contents in the bedrock layers at larger depths, which exert no large cooling effect on the surface from below during thawing. However, this approach clearly neglects all long-term effects of past climatic conditions on the ground thermal regime at larger depths. Therefore, simulation results at larger depths should not be interpreted in a climate context.

4 Calibration procedure: GLUE

With the recent increase in computing power, the automation of the calibration of soil models, also called inverse modelling, has been used increasingly (e.g. Finsterle et al., 2012; Cui et al., 2011; Boeckli et al., 2012; Tonkin et Doherty, 2009). This method can handle complex systems with a large number of free parameters, and calibrate them using on-site measured data. Among the many statistical methods available, the Generalized Likelihood Uncertainty Estimation (GLUE), developed by Beven and Binley (1992), is implemented in the CoupModel (Jansson, 2012) and has been used in the present study. GLUE assesses the equivalence of a large number of different parameter set-ups stochastically selected among a given set of parameter value ranges. It is based on the premise that any model set-up is, to a certain extent, in error with reality (Morton, 1993). Assigning a likelihood to any model set-up will allow the selection of the most correct one within the number of tested sets of model parameters. The probability of getting a result with reasonable likelihood increases with the number of simulations, especially for a complex system with a large number of parameters. Expert knowledge of the system is required (a) to select the parameters to test and (b) to define their ranges in order to minimize the error sources resulting from physically intercorrelated parameters, autocorrelation, insensitive parameters and heteroscedasticity (sub-populations that have different variabilities from others that invalidate statistical tests) in the residuals (Beven and Binley, 1992). However, a large

Table 2. List of parameters used in the GLUE calibration method and their corresponding equations.

Parameter	Description	Range tested	Equation(s) related
T_{rain}	Threshold temperature in the partition of precipitation into rain and snow. Above this value, precipitation only falls in liquid form.	0.1 to 4 (°C)	$Q_{\mathrm{P}} = \begin{cases} \min\left(1, (1 - f_{\mathrm{liqmax}}) + f_{\mathrm{liqmax}} \dfrac{T_{\mathrm{a}} - T_{\mathrm{rain}}}{T_{\mathrm{snow}} - T_{\mathrm{rain}}}\right), & T_{\mathrm{a}} \leq T_{\mathrm{rain}} \\ 0, & T_{\mathrm{a}} > T_{\mathrm{rain}} \end{cases}$
T_{snow}	Threshold temperature in the partition of precipitation into rain and snow. Under this value, precipitation only falls in solid form.	−5 to 0 (°C)	
ρ_{snowmin}	Density of new snow. Used in the function determining the density of the whole snow pack (new and old snow).	50 to 200 ($\mathrm{kg\,m^{-3}}$)	$\rho_{\mathrm{snow}} = \frac{\rho_{\mathrm{snowmin}}}{119.17 f_{\mathrm{liqmax}}} \left(67.92 + 51.25 e^{\frac{T_{\mathrm{a}}}{2.59}}\right)$
S_k	Coefficient used in calculation of the thermal conductivity of snow.	10^{-7} to 10^{-5}	$k_{\mathrm{snow}} = S_k \rho_{\mathrm{snow}}^2$
$\mathrm{Melt_{rad}}$	Coefficient used to tune the importance of the global radiation on the empirical snowmelt function.	0 to 3×10^{-6}	$M_{\mathrm{R}} = \mathrm{Melt_{rad}} \left(1 + s_1 \left(1 - e^{-s_2 2}\right)\right)$ $\mathrm{Melt_{temp}} = \begin{cases} \mathrm{Melt_{temp}} & T_{\mathrm{a}} \geq 0 \\ \dfrac{\mathrm{Melt_{temp}}}{\Delta z_{\mathrm{snow}} m_f} & T_{\mathrm{a}} < 0 \end{cases}$
$\mathrm{Melt_{temp}}$	Coefficient used to tune the importance of air temperature on the empirical snowmelt function.	0.5 to 4	$M = \mathrm{Melt_{temp}} T_{\mathrm{a}} + \mathrm{Melt_{rad}} R_{is} + \frac{f_{q_{\mathrm{h}}} q_{\mathrm{h}}(0)}{L_{\mathrm{f}}}$
ΔS_{crit}	Threshold snow height parameter for the soil to be considered as completely covered by snow. It is used to calculate the fraction of bare soil during patchy snow conditions by weighting the sum of temperature below the snow and the temperature of bare soil.	0.1 to 2 (m)	$\mathrm{f_{bare}} = \begin{cases} \dfrac{\Delta z_{\mathrm{snow}}}{\Delta S_{\mathrm{crit}}} & \Delta z_{\mathrm{snow}} < \Delta S_{\mathrm{crit}} \\ 0 & \Delta z_{\mathrm{snow}} \geq \Delta z_{\mathrm{cov}} \end{cases}$
$\alpha_{\mathrm{dry}}, \alpha_{\mathrm{wet}}$	Albedo of dry/wet soil. This parameter is used to define the albedo function of the soil to calculate the net radiation.	10 to 40 (%)	$R_{\mathrm{snet}} = R_{is}(1 - \alpha)$
ψ_{eg}	Factor to account for differences between water tension in the middle of top layer and actual vapour pressure at the soil surface in the calculation of the energy balance at the soil surface.	0 to 3	$L_{\mathrm{v}} = \frac{\rho_{\mathrm{a}} c_p}{\gamma} \frac{(e_{\mathrm{surf}} - e_{\mathrm{a}})}{r_{a_{\mathrm{s}}}}$ $e_{\mathrm{surf}} = e_{\mathrm{s}}(T_{\mathrm{s}})\, e^{\left(\frac{-\Psi_1 M_{\mathrm{water}} g e_{\mathrm{corr}}}{R(T_{\mathrm{s}} + T_{\mathrm{abszero}})}\right)}$ $e_{\mathrm{corr}} = 10^{\left(-\delta_{\mathrm{surf}} \Psi_{\mathrm{eg}}\right)}$
k_w	Saturated hydraulic conductivity. This parameter is also used in the calculation of the unsaturated hydraulic conductivity.	100 to 10^5 ($\mathrm{mm\,day^{-1}}$)	$k_{\mathrm{tot}} = k_w S_{\mathrm{e}}^{\left(n + 2 + \frac{2}{\lambda}\right)}$
g_m	Empirical parameter used in the water retention function, in the effective saturation particularly.	0.1 to 2	$S_{\mathrm{e}} = \frac{1}{(1 + (\alpha \Psi)^{g_n})^{g_m}}$
Φ	Porosity, used in the water content calculation.	site-specific (%)	$\theta = S_{\mathrm{e}} \left(\Phi - \theta_y\right) + \theta_{\mathrm{r}}$
K_{soil}	Multiplicative scaling coefficient for the thermal conductivity applicable for each soil layer. This value is multiplied with the thermal conductivity calculated from Kerten's equation for unfrozen and frozen soils.	−0.5 to 0.5	$k_{\mathrm{unfrozen}} = h_1 + h_2 \theta$ $k_{\mathrm{frozen}} = b_1 10^{b_2 \rho_{\mathrm{s}}} + b_3 \left(\frac{\theta}{\rho_{\mathrm{s}}}\right) 10^{b_4 \rho_{\mathrm{s}}}$

number of simulations with different sets of parameters may also raise the equifinality problem: several model set-ups can lead to an acceptable calibration (Beven and Freer, 2001), which may lead to uncertainty in the prediction. For example, two model set-ups giving the same likelihood during the calibration process could lead to different results when used for long-term simulations.

In addition, a model set-up that is consistent with present-day conditions may not be optimal for future climatic conditions. This well-known problem is inherent to most long-term transient simulations with a high number of parameterized and calibrated processes. One possibility to avoid compensation of two or several parameters showing unphysical or unrealistic values is to (i) constrain the parameter range to physical plausible values and (ii) verify whether the obtained calibration values for all parameters contain any outliers, which cannot be explained by site-specific conditions. However, it has to be noted that the aim of the calibration procedure is not the determination of the parameter values (e.g. physical properties) themselves, but to get a model that is thermally most representative for the ground thermal regime at a given site. Keeping the above constraints in mind, for long-term simulations, where no observations are available, it has to be assumed that the parameters governing the ground thermal regime do not change significantly over the duration of the simulation.

We selected 14 parameters that have either shown a large influence on modelled temperature variations in previous studies and/or are known to be important in reality (cf. Lütschg et al., 2008; Schneider et al., 2012; Scherler et al., 2013, 2014; Gubler et al., 2013; Marmy et al., 2013). The 14 parameters (listed in Table 2) were tested for each site in a first iteration of 50 000 simulations. Each of the simulations was run with stochastically selected parameter values, thus creating 50 000 different model set-ups. The most sensitive model parameters were then identified for each site based on their relative importance on calibration performance (Figs. 4 and 5). Those four to six sensitive parameters were then used in a second iteration of 20 000 simulations to refine the calibration. It is important to note that the sensitive parameters may differ from site to site depending on site-specific characteristics, although initial parameters and their ranges were equivalent for all sites (see next section). From the 20 000 simulations of the second GLUE calibration iteration, an optimal model set-up for each site was then selected based on statistical performance indicators (r^2 and the mean error, ME) for ground temperature at several depths. The calibration procedure is summarized in Fig. 4. In addition to useful information about site-specific processes and their representation in the model (see next section), the calibration obtained by this method led to the selection of a model set-up for the long-term simulations forced by the GCM/RCM data.

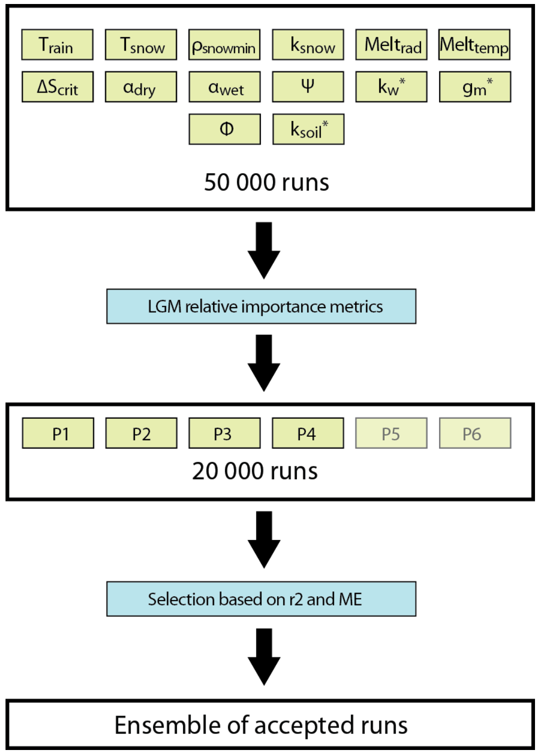

Figure 4. Calibration procedure using the GLUE method in the following steps: **(a)** first iteration, stochastically testing 14 different parameters in 50 000 runs, **(b)** selection of the most sensitive parameters for each site using the LGM method, **(c)** refinement of the calibration with a second iteration of 20 000 runs focusing on the four to six sensitive parameters (may be different for each site), **(d)** selection of acceptable model set-ups among the 20 000 simulations based on statistical performance indicators (r^2 and the mean error, ME) for ground temperature at several depths. Among those four to six set-ups, the median (regarding the evolution of active layer thickness) is eventually used for long-term simulations.

5 Calibration results

5.1 Relative importance metrics

The GLUE method was used to test a large number of parameters at each site and to statistically assess their relative importance in the model. The relative importance of each parameter in the model is calculated based on the standardized covariance matrix of the tested parameters and related model performances using the LGM (Lindeman, Gold and Merenda) method (Lindeman et al., 1980) that averages the sequential sums of squares over all orderings of regressors. We group the parameters into six categories: (1) snow parameters (T_{rain}, T_{snow}, ρ_{snowmin}, S_k, $\mathrm{Melt}_{\mathrm{rad}}$, $\mathrm{Melt}_{\mathrm{temp}}$, ΔS_{crit}), (2) albedo parameters (α_{dry}, α_{wet}), (3) hydraulic conductivity (k_w, g_m), (4) porosity (Φ), (5) thermal conductivity (K_{soil}) and (6) evaporation (ψ_{eg}), and evaluate the influence of each parameter group on the statistical performance indicators r^2

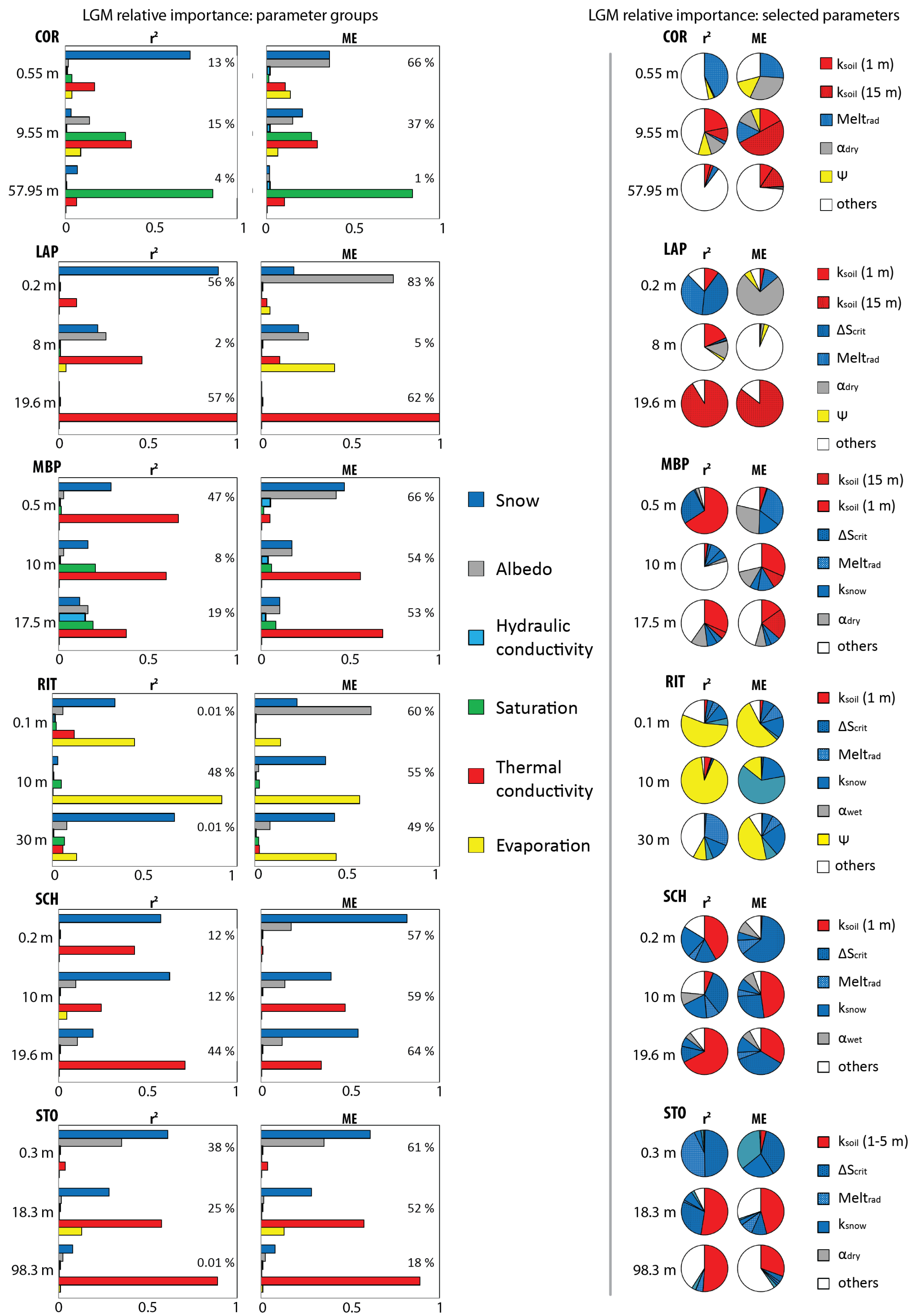

Figure 5. Left panel: LGM relative importance of six groups of parameters (snow, albedo, hydraulic conductivity, saturation, thermal conductivity and evaporation) on the r^2 (left row) and the ME (right row) at three different depths. The percentage indicates the total LGM absolute importance. Right panel: LGM relative importance of the most sensitive parameters that were selected for the second step of the calibration procedure.

and ME at three different depths (near-surface, around 10 m, and the maximal depth of each borehole). The r^2 accounts for variance, whereas ME accounts for absolute errors. This joint analysis of correlation and mean error is needed, as small temperature biases near the freezing point may result in large errors when latent heat processes are not adequately represented. While minimizing the ME ensures that the absolute values are near the observed ones, the correct simulation of the timing of freeze/thaw events can be improved by maximizing the correlation coefficient. It is clear that in the case of long-lasting freeze/thaw events, a good correlation will always be difficult to achieve, but a reasonable good match was achieved at least for the near-surface layers by optimizing the correlation. In a future step, other quantities such as the energy content of the ground (Jafarov et al., 2012) could be used for calibration, but variables directly related to the amount of water present (see Sect. 7) can also be used to enhance the calibration.

The results of the calibration are shown in Fig. 5 (left panels). Hereby, the relative importance of the six groups of parameters are shown for the three different depths as well as the absolute importance of the varying parameters on the simulations results (in %). A large relative importance identifies a parameter or process as being dominant with respect to the other parameter groups; however, it can still have a low overall importance on the simulation results, if the absolute importance is low.

As already noted in many previous studies (e.g. Lütschg et al., 2008; Gubler et al., 2013; Scherler et al., 2013; Atchley et al., 2016), Fig. 5 shows that the snow parameters have the greatest importance on the calibration performance for all sites. This importance is obviously pronounced at the surface, as the snow conditions represent a large part of the upper boundary condition by influencing the ground surface temperature during the snow-covered period. The variation of r^2 at the surface is explained by snow with a relative importance usually above 50 %, ranging from 34 % at RIT up to 72 % at COR and 90 % at LAP. The differences between the sites can be explained by different snow conditions: there is a mean of about 280 days with snow cover per year at RIT, whereas COR only has about 200 days of snow cover days per year, indicating that the relative importance of snow for model calibration decreases with increasing snow cover. Hence a site with long and thick snow cover is less sensitive to variations in the snow parameters, as the snow persists anyway during a long period, than sites with less snow and a faster transition between snow-covered and snow-free ground. At LAP, snow cover conditions are additionally influenced by the presence of ski tracks and frequent occurrence of avalanches (cf. Staub et al., 2015).

In comparison with r^2, ME is less influenced by snow parameters, as snow cover is more important for seasonal temperature variability (i.e. by accurately reproducing the transition between snow-covered and snow-free ground) than for absolute temperatures values. Interestingly, the relative influence of snow on ground temperatures is still large at greater depths: snow explains 12 % of the r^2 and 10 % of the ME at MBP at 17.5; 65 % of the r^2 and 43 % of the ME at RIT at 30 m, 19 % of the r^2 and 54 % of the ME at SCH at 13.7 m; 8 % of the r^2 and 8 % of the ME at STO at 98.3 m. At 57.95 m at COR, the snow shows a very limited influence as it explains only 0.1 % of the r^2 and 0 % of the ME at this depth. This is probably related to the thick model layer with high porosity (cf. Fig. 3), where massive ice is permanently present, which decouples the lowest layers from processes at the upper boundary.

The albedo parameters have a significant influence on the calibration results at all sites, with relative importance for the ME ranging from 17 % at SCH to 74 % at LAP, reflecting the calibration of the surface temperature amplitudes. The r^2 (reflecting the inter-seasonal variation) is less or not influenced by the albedo. In some cases at greater depths (r^2 and ME at 10 m at COR, 8 m at LAP), albedo appears to have a high relative influence, sometimes higher than at the surface. This is most likely not related to realistic physical processes: intermediate depths, which are located between the well-calibrated upper and lower boundary conditions, are difficult to calibrate with any of the parameters tested (see the low percentages of absolute importance in Fig. 5). Therefore, those values are interpreted as statistical artefacts.

The sum of the influence of snow, albedo and evaporation parameters ranges from 58 (SCH) to 100 % (RIT) near the surface, from 26 % (COR) to 97 % (RIT) at medium depth and from 7 (STO) to 96 % (RIT) at larger depths for r^2. This highlights the major role played by the upper boundary condition in the calibration. LAP and COR are exceptions as the importance of the upper boundary parameters is high at the surface (90 % for r^2 and 97 % for ME at LAP and 78 % for r^2 and 86 % of the ME at COR) but negligible at larger depths, where variation of r^2 and ME is mainly due to variation of the thermal conductivity. The model needs to broadly tune the thermal conductivities (between 0.3 and 2.5 W m^{-1} K^{-1}) of certain layers (10–15 m) to correct the temperature where a missing process or an incorrect soil structure parameterization need to be corrected. LAP and COR are two ice-rich sites (as seen e.g. in the geophysical results by Hilbich, 2009; Hilbich et al., 2009), with large blocks at the surface and high porosity. The combination of these effects decouples the intermediate layers from the upper boundary conditions to a larger extent than at MBP and RIT, which are also sites with coarse-grained material, but with a smaller estimated porosity by the model (Fig. 3).

Not surprisingly, the thermal conductivity plays a large role at depth where the relative importance (ME) ranges from 34 % at SCH to 89 % at STO and even 100 % at LAP (an exception is COR with 11 %). At MBP, thermal conductivity plays a large role even at the surface (67 % of the r^2). As mentioned above, a potential radiation bias could be present in the input data of MBP due to the absence of on-site measured global radiation. A compensation of a potential bias would be expected either in the near-surface thermal conductivities or in the albedo values. Although the critical snow height parameter ΔS_{crit} for MBP is very low, indicating a potential model compensation as it affects the albedo calculation, the albedo values themselves were calibrated with average values ($\alpha_{\text{dry}} = 24.1\,\%$, $\alpha_{\text{wet}} = 19.1\,\%$), which rather points to the absence of a large radiation bias. Similarly, the calibrated thermal conductivity values for the near-surface layer are about average (around 2–4 $\text{W m}^{-1}\,\text{K}^{-1}$) compared to the other sites and do not indicate a large bias towards radiation-based surface temperatures that are too warm.

Among all sites, only RIT is insensitive to changes in the thermal conductivity (3 % of ME at 30 m depth). On the other hand, evaporation has a strong influence on calibration even at larger depths (44 %), which is in strong contrast to all other sites, where this parameter shows only little influence (between 0 and 10 %). When analysing the specific values obtained for the different calibration parameters, the parameter related to evaporation (water tension Ψ_{eg}, cf. Table 2) did not show specifically high or low values for RIT, but the parameterized values for T_{snow} (minimum temperature at which precipitation only falls as snow) and ΔS_{crit} (critical snow depth, at which the whole surface is considered to be covered by snow) were very low ($T_{\text{snow}} = -4.86\,°\text{C}$) and high ($\Delta S_{\text{crit}} = 1.9\,\text{m}$), respectively. Whereas the former leads to comparatively large precipitation input as rain, the latter leads to an almost never completely snow-covered surface. In addition, the wet soil albedo for RIT is calibrated with the lowest value of all sites ($\alpha_{\text{wet}} = 7.0$), whereas its dry albedo is comparatively high ($\alpha_{\text{dry}} = 34.6$). In total, this parameter combination enables additional energy input by liquid water into the subsurface, which of course also explains the high sensitivity to evaporation. Even though this parameter combination may lead to an unrealistic process representation in the model, it is still in good accordance with observations, as at RIT the effect of 3-D advective water flow from the melting snow cover has been observed in borehole temperatures (Zenklusen Mutter and Phillips, 2012; Luethi et al., 2016), which explains this specific calibration outcome. Of course, the real 3-D process of meltwater infiltration cannot be explicitly included in our model.

Porosity and hydraulic conductivity of different horizons show little or no influence on calibration performance. For porosity this is not surprising as the parameter ranges are narrow to keep porosity close to reality. The only site showing sensitivity of changes in porosity is MBP (20 % of importance for the r^2 at 10 m and 19 % at 17.5 m), which is specifically sensitive to changes of the porosity of the second soil layer (1.6 to 3.6 m depth). This points to an imprecise initial soil structure set-up that the model needed to correct, in this case the thickness of the surface blocky layer with high porosity.

When considering the absolute importance (% in Fig. 5, left panels), we notice that deep boreholes (COR, RIT and STO) have low percentages, which is not surprising as the temperatures at those depths vary on much longer timescales and depend primarily on the structural set-up of the model. As their future evolution is influenced by past climates, which are not included in the present study, simulated temperature changes at large depths will not be discussed within this study. However, their correct representation for present-day climate is important as the lower boundary condition for shallower levels. Contrary to these deep levels, the surface at all sites shows the highest sensitivity to the tested parameters, due mainly, as explained above, to the high importance of snow and albedo parameters.

After the LGM analysis, the most sensitive parameters for each site were identified to be used in the second iteration of the GLUE calibration procedure (cf. Fig. 4) to refine the calibration. The parameters listed in Fig. 5 (right panels) are the four to six most important parameters in the variation of statistical indicators; their relative importance for the variation of r^2 and ME at three different depths is represented by the pie charts. One parameter that shows high sensitivity is ΔS_{crit}, which allows the model to correct for the imprecise snow conditions and systematic biases in the building of the snow cover. The biases regarding the disappearance of the snow cover in early summer are corrected by the parameter Melt_{rad} (coefficient for the importance of global radiation in the melt function of the snow). The thermal conductivity (k_{soil}) is important to adjust temperatures at middle and lower depth (COR, LAP, SCH and STO) but also at the surface (MBP). It can also be seen that snow parameters (blue colours in the pie diagrams) have stronger influence at the two bedrock sites (SCH, STO) compared to talus slopes and rock glaciers (COR, MBP, RIT, LAP), where other processes such as advection, convection and latent heat processes (due to the higher ice content) play a major role at depth.

5.2 Ground temperatures

To identify the most accurate runs among the 20 000 runs of the second iteration, we apply a selection based on two balanced criteria: (i) selecting the runs with the highest r^2 (i.e. seasonal and interannual variability) in layers close to the surface and (ii) reducing the ME as much as possible (i.e. model temperature bias, leading to a model that is too warm or too cold globally) at greater depth. This option has been preferred over a globally best r^2 or ME averaged over all depths because the latter would put the weight equally to all depths, whereas the surface is more important (and more accurate) regarding decadal changes.

Figure 6 shows the performance of the calibration at each site for three different depths, indicating the obtained value of r^2 and ME. It has to be pointed out that a low r^2 or high ME value does not mean that a better result at a certain depth cannot be obtained by GLUE because the selection process is a compromise between r^2 and ME at several depths. Most calibration runs produce either well-calibrated temperatures

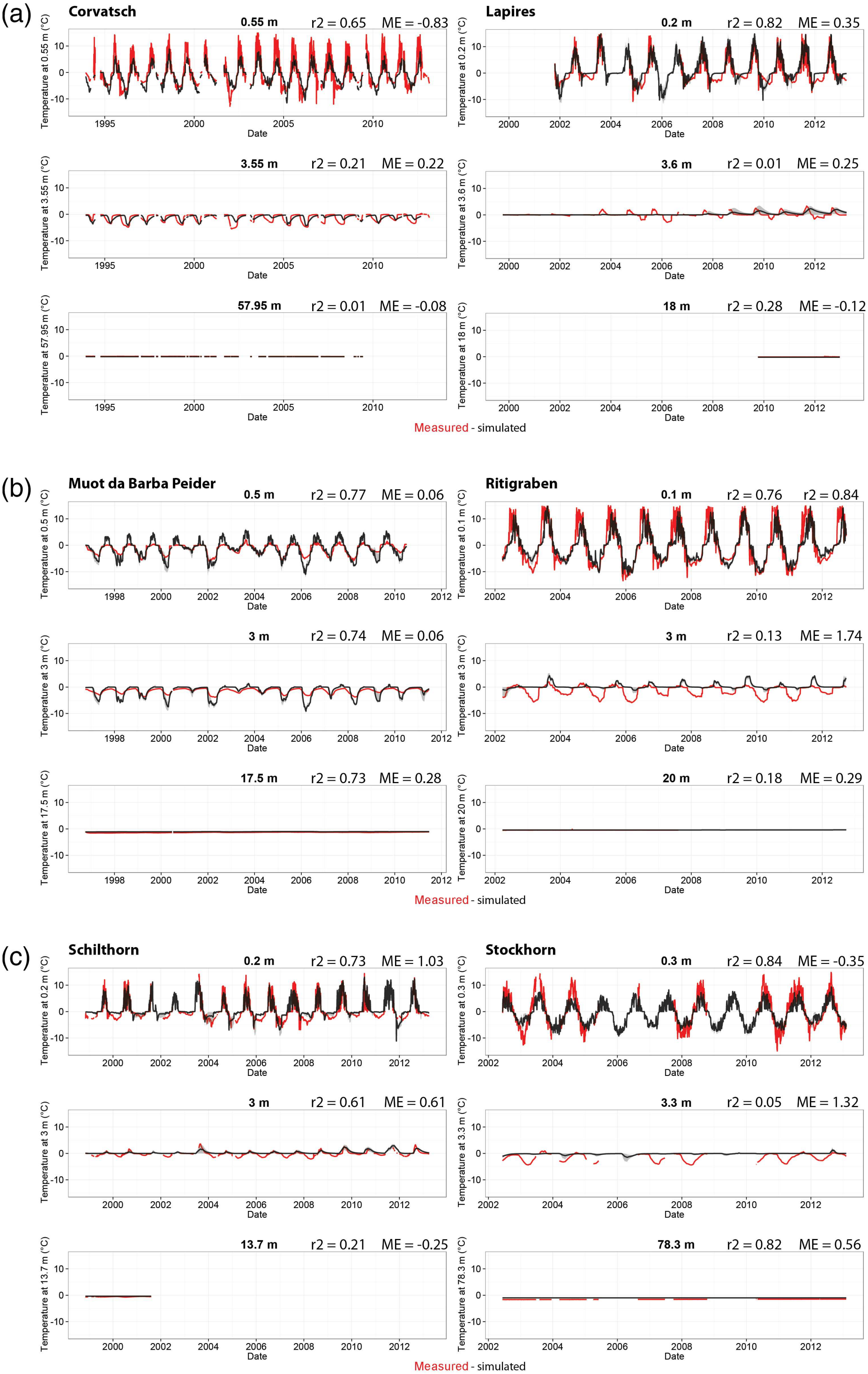

Figure 6. **(a)** Comparison of simulated (black) and measured (red) temperature during the calibration period at six sites at three different depths: one close to the surface, one around 3 m and one close to the lower boundary of the model for Corvatsch and Lapires. **(b)** As in **(a)** but for Muot da Barba Peider and Ritigraben. **(c)** As in **(a)** but for Schilthorn and Stockhorn.

near the surface or at greater depths, but not both for the same set of calibration parameter.

Calibration at the surface is very good at LAP and STO ($r^2 > 0.8$), indicating a good representation of the upper boundary condition, especially regarding snow timing and duration. At the four other sites, r^2 at the surface ranges between 0.65 (COR) and 0.77 (MBP). The comparatively low values at COR are not surprising due to the presence of very coarse blocks (> 2 m) at the surface inducing additional processes in the active layer that influence the near-surface sensors in the borehole (Scherler et al., 2014). The general variation and absolute values of near-surface ground temperature are satisfactory. Some systematic mismatches exist, such as insufficient cooling during winter at SCH and LAP, or excessive cooling in winter at MBP. At MBP, this is compensated by an equally high excessive warming during summer. At STO, the general behaviour of the near-surface temperature is accurately reproduced by the calibration, but with a reduced amplitude (warmer in winter and cooler in summer). At COR, there is an insufficient warming in summer, leading to a negative bias at the surface.

Temperatures at or around 3 m are the most challenging to calibrate as the influences of the upper and the lower boundary conditions have to be balanced. Moreover, this depth is usually within the active layer, and a small error in temperature (and/or soil water content) will lead to a mismatch in active layer thickness (e.g. at STO). Without putting a specific focus on matching the active layer thickness, the transition between frozen and unfrozen conditions is difficult to reproduce, especially given that subsurface structure and composition is generally unknown. The selection process showed that the selection of the best r^2 at this depth led to the introduction of a strong positive bias in the absolute value (leading to disappearance of permafrost) and to poor calibration results at lower depth. A reduction of the ME at this depth led to a better representation of the permafrost conditions at all sites, but as a consequence the seasonal variations at this depth could not always be reproduced.

Seasonal variations at this depth are only reproduced correctly at MBP (low ME and high r^2) and, to a certain extent, at COR and SCH (cf. Fig. 6). At SCH a warm bias is introduced in the model at 3 m depth, which can be explained by insufficient cooling during winter at the surface which propagates to larger depths. At COR, the warm bias at the surface is not reproduced at 3.55 m due to the permafrost conditions at this depth in the model. At RIT and STO, the model shows a constant temperature at the freezing point, leading to a large positive bias (1.74 K at RIT and 1.32 K at STO). At LAP, the model also shows temperatures at the freezing point at 3.6 m, and it is only able to reproduce some seasonal variations at the end of the calibration period. The bias at LAP is slightly positive (0.25 K).

Calibration of the lowermost layer is always satisfactory even though the model shows a small positive bias at STO (0.56 K), RIT (0.29 K) (probably originating from the propagation of the warm bias at 3 m) and MBP (0.28 K), and a negative bias at SCH (−0.25 K). Even if the calibration resulting from the GLUE procedure is not always satisfactory, it represents the optimal set-up for the given initial model for each site under the constraints of the semi-automated calibration approach presented in this study.

6 Long-term simulations

One of the goals of any calibration is to obtain a suitable set of model parameters to be used in further analysis. The TEMPS project had the overall goal to investigate the present and possible long-term evolution of mountain permafrost in Switzerland. Hence, the calibrated model set-ups for each site were forced with downscaled and bias-corrected climate model output data from 13 GCM/RCM chains as explained in Sect. 3.1. The corresponding changes of the two main meteorological driving variables, air temperature (see Fig. 2) and precipitation, are summarized in Table 3.

Figure 7 shows the simulated evolution of ground temperature at 10 and 20 m, both as mean of 13 scenario simulations for each site as well as the corresponding ensemble range. The chosen depths show permanently frozen conditions during the observation period (cf. PERMOS, 2016) but are subject to thaw in a climate warming perspective. Because the calibration procedure identified implausible combinations of parameter values for RIT (due to 3-D advective processes as described by Luethi et al., 2016), which may lead to erroneous projections for the future, no long-term projections are shown for this site.

At all sites, the 10 m layer is projected to be unfrozen by the end of the century, but there is a considerable difference regarding the timing between the sites. Moreover, there is uncertainty among the 13 different GCM/RCM chains (grey area in Fig. 7). The 10 m layer is projected to become unfrozen between the decades 2060 and 2090 at COR, 2030 and 2060 at LAP, 2020 and 2030 at SCH and 2010 to 2060 at STO. At MBP, the 10 m layer is projected to be unfrozen by 2080 for certain chains but remains frozen until the end of the century for other chains.

Once its ice has permanently melted, the 10 m layer is subject to significant seasonal variations (see COR, RIT and STO). SCH is not affected by the seasonal variations as much, though the layer is projected to be unfrozen early in the century because of a smaller decrease in snow cover duration in comparison with other sites. In addition, its permafrost degradation is less pronounced than projected in Scherler et al. (2013). This is most probably due to the cold bias introduced during the calibration and to a slightly higher porosity value at depth (7 % as opposed to 5 % in Scherler et al., 2013), leading to higher ice content and therefore a slower degradation. Note as well that the air temperature warming at SCH is the lowest (+3.36 K, see Table 3) compared to other sites. At LAP, COR and MBP, the soil is pro-

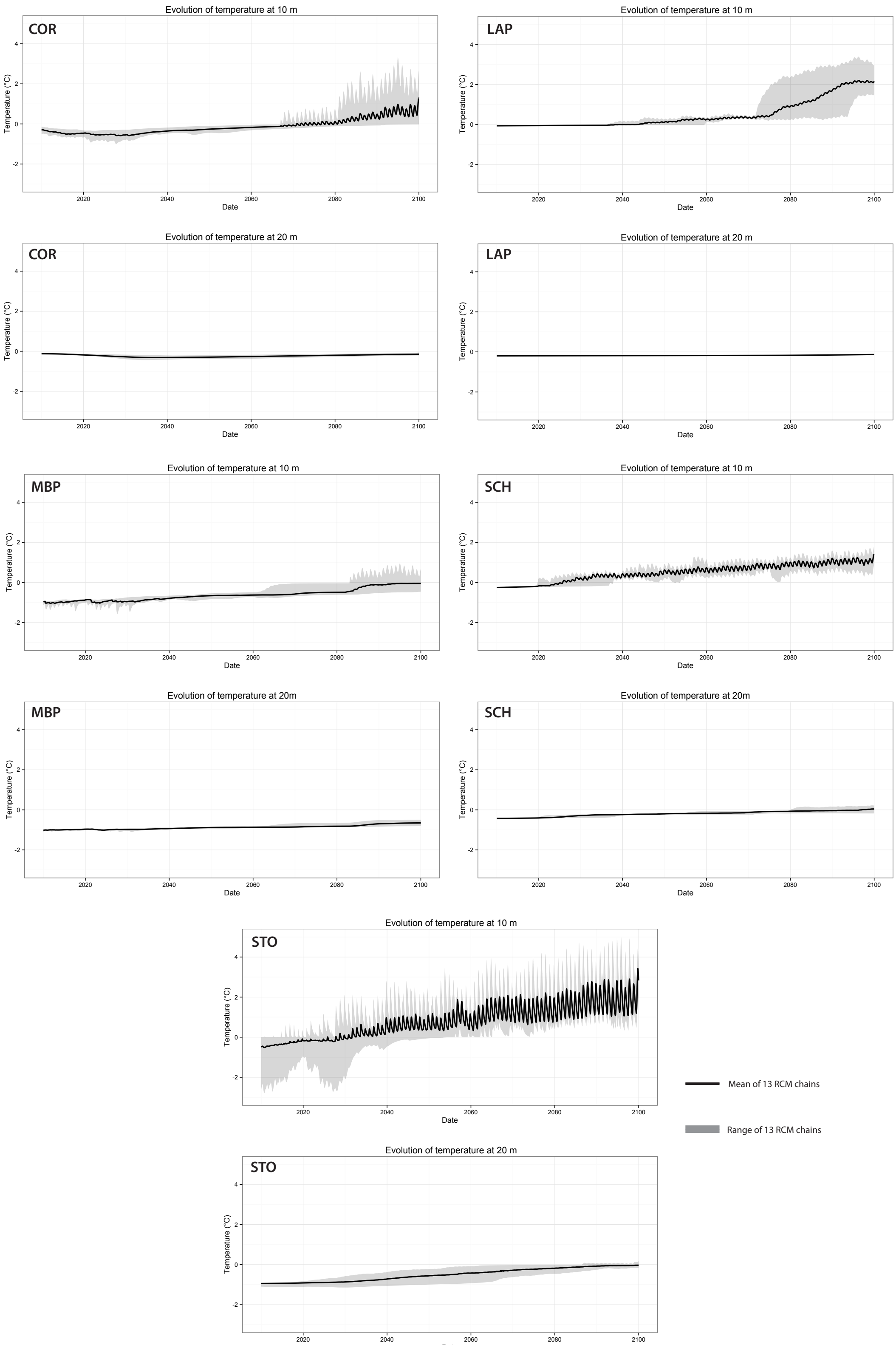

Figure 7. Long-term evolution of ground temperatures at 10 and 20 m as simulated by the CoupModel for the different sites. The black lines represent the median scenario and the grey zone the range of the 13 GCM/RCM chains.

Table 3. Summary of changes projected for two different decades (2040–2049 and 2090–2099): mean of 13 GCM/RCM chains for change in mean air temperature, in mean precipitation sum and in simulated snow cover duration (number of days per year with snow 0.1 m) compared to the 2000–2010 decade.

	Δair T (K)		Δprec (%)		Δdays of snow (%)	
	2040–2049	2090–2099	2040–2049	2090–2099	2040–2049	2090–2099
Corvatsch	+1.58 +1.05/+2.11	+3.97 +3.14/+5.38	+8.4 +0.31/+18.18	+4.4 −10.26/+16.43	−10.84 −18.77/+6.74	−23.75 −45.42/−4.91
Lapires	+1.67 +0.99/+2.15	+4.23 +3.04/+5.83	+0.63 −6.54/+9.28	−0.82 −22.87/−8.24	−16.73 −23.67/−8.00	−37.06 −57.28/−27.88
Muot da Barba Peider	+1.58 +1.05/+2.10	+3.95 +3.13/5.33	+10.24 +0.64/21.48	+6.74 −8.79/+18.27	−8.63 −11.94/−4.13	−22.81 −37.11/−8.03
Ritigraben	+1.62 +0.97/2.08	+4.10 +2.95/+5.65	+2.14 −4.98/+11.64	+4.89 −20.25/+14.68	−14.76 −20.32/−5.93	−32.31 −49.42/−20.57
Schilthorn	+1.40 +0.92/+1.91	+3.36 +2.30/4.35	−1.20 −8.50/+6.51	−2.72 −16.78/+11.33	−9.21 −12.24/−4.27	−20.03 −35.73/−12.09
Stockhorn	+1.55 +0.96/+2.00	+3.86 +2.84/+5.31	+2.08 −5.61/+11.33	+4.68 −20.01/+14.69	−10.23 −14.18/−5.35	−24.59 −39.53/−16.33

jected to remain frozen at 20 m until the end of the century. At SCH and STO, some chains project a thawing, occurring around 2080–2090, while other chains project negative temperatures at 20 m until the end of the century.

As mentioned above, the snow cover duration is one key element for the evolution of the ground thermal regime. Its evolution in the future is expected to be mostly influenced by changes in air temperature: the changes in the annual sum of precipitation are highly uncertain and do not generally exceed ±5 % in the GCM/RCM output (see Table 3; but with high variability among the chains), while the simulated mean change in snow cover duration ranges from −20 % (SCH) to −37 % (LAP). Figure 8 shows the relationship between the air temperature increase and the decrease in snow cover duration. For all sites, the correlation is linear and the trend of snow cover duration decrease per degree of warming ranges from $-5.98\,\mathrm{days\,K^{-1}}$ (COR) to $-8.76\,\mathrm{days\,K^{-1}}$ (LAP). This decrease represents a shortening of the snow cover duration of 48 days (COR) to 88 days (LAP) until the end of the century. The range of the different GCM/RCM chains is broad, confirming the high uncertainty and the general difficulty in projecting the evolution of precipitation.

7 Discussion

7.1 Approach

The GLUE calibration method is not meant to determine the physical value of a parameter. The model is physically based regarding its underlying equations, but has to rely on parameterizations for many of the complex processes in the subsurface and at the soil–snow–atmosphere boundary. The values for all model parameters at all depths cannot be known exactly, especially as almost no direct measurements of these properties are available. The GLUE method enables the value that gives the best fit with observations within the number of tested runs to be found. However, as the system is complex, with sometimes highly uncertain initial and boundary conditions, non-linear processes and simplifications of the model structure make an optimum calibration impossible (Beven, 2002). It is therefore more meaningful to analyse the residuals and the sensitivity to parameters than the values of the parameter themselves.

The calibration with GLUE depends on several subjective initial assumptions: (a) the choice of tested parameters and their range; this choice has to be made by the modeller prior to the calibration, and is a result of previous tests to identify relevant and sensitive parameters, and (b) the choice of criteria of acceptance. For the former, we tried to include a representative set of parameters for surface processes (snow, albedo, evaporation), subsurface processes (thermal and hydraulic conductivity) and properties that are characteristic of the specific geomorphological sites (porosity) in order to provide enough degrees of freedom for a satisfactory calibration. In addition we used our prior experience with CoupModel (cf. Engelhardt et al., 2010; Scherler et al., 2010, 2013, 2014; Marmy et al., 2014; Staub et al., 2015) to identify the most sensitive parameters. We tried to fix the allowed parameter range to physically plausible ranges, and verified that the obtained values during calibration were not distributed at the limits of these ranges. Regarding the choice of criteria of acceptance, we gave priority to good correlation coefficients near the surface and at intermediate levels while making sure that mean errors were acceptable at all depths. Here, different simulation results would have been obtained by e.g. giving more weight to intermediate levels; however,

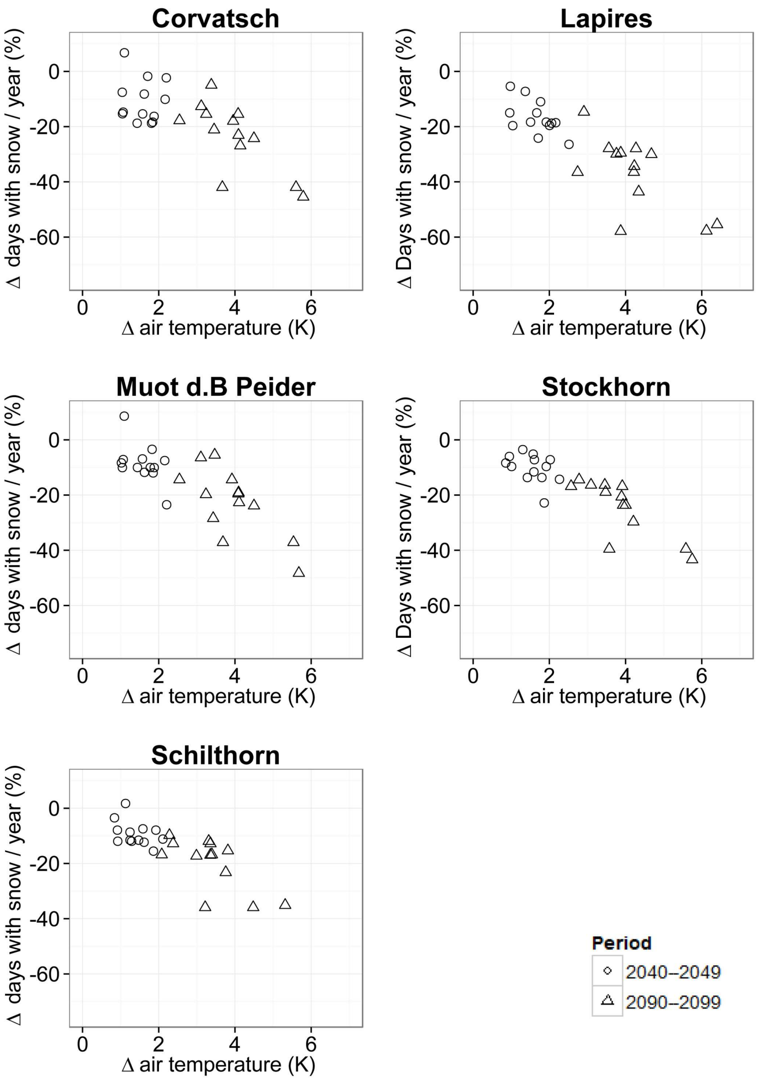

Figure 8. Relationship between the decreasing snow duration and the increase of air temperature for the decades 2040–2049 (dots, representing the 10-year means Δ for each GCM/RCM chain) and 2090–2099 (triangles, representing the 10-year means Δ for each GCM/RCM chain), in comparison with the decade 2000–2010. The trend is variable between the sites (from -5.29 to $-8.76\,\%\,K^{-1}$), but all sites show a linear correlation between Δ air temperature and reduction of days with snow.

due to the uncertainties regarding the influence of past climates at the lower boundary, and regarding the exact representation of temperature evolution near the freezing point, the results would be less certain than in the case of a well-calibrated model at the upper boundary. Finally, uncertainties of the calibration add themselves to the uncertainties of observation and climate models when considering the long-term simulations.

7.2 Calibration

One challenge of the calibration with GLUE is that there are many parameters to calibrate that are often underdetermined with respect to the available data. Therefore, the optimum is sometimes poorly defined, especially for sites that include processes like 2-D air circulation, which is not taken into account in the present model formulation. According to Beven (2002), an increased physical realism of the model structure does not aid in obtaining a better calibration. The perfect model would include an extremely large number of parameters and be unique to each site, and this is of course unrealistic.

In comparison with other permafrost modelling studies (e.g. Scherler et al., 2013; Westermann et al., 2013; Fiddes et al., 2015), the calibration method reaches a satisfactory calibration level for most of the sites. The obtained biases in the calibration may originate from several phenomena (which are very likely linked): (a) neglect of a sensitive model parameter in the calibration process, (b) parameter ranges that are too narrow, which do not allow the global optimum to be reached, (c) insufficient number of runs to find the optimum for each site, (d) errors regarding the initial model structure (soil type, horizons, etc.), (e) biases introduced in the reconstruction of the input meteorological data or (f) errors or imprecision in temperature measurements.

In addition, several potentially relevant processes such as convective flow of air in the coarse blocky layer or 2-D air or water circulation are not included explicitly in the CoupModel. In a previous study, this was solved by artificially creating a heat source/sink to reproduce convection within the coarse blocky layer of rock glacier Murtèl (Scherler et al., 2013). A similar parameterization for advective water flow within the SNOWPACK model has been published by Luethi et al. (2016) for Ritigraben.

Other processes that were not taken into account in the model concern the snow redistribution by avalanches or by wind that often takes place in high mountain environments (Hoelzle et al., 2001; Lehning et al., 2008; Mott et al., 2010; Gisnås et al., 2016). However, we could quantify the influence of several snow parameters. Snow has an especially strong influence at sites with shorter snow cover duration: there it is the most important parameter for the variations at the surface, but it also has a strong influence at deeper layers. The sites with a long-lasting snow cover (RIT and MBP) showed a reduced sensitivity to snow parameters as the snow is present most of the time, and the transition between snow-covered and snow-free conditions is less difficult to simulate. In general, the definition of the upper boundary conditions (snow, albedo, evaporation) appears to be a crucial issue as they influence the performance of the calibration of the whole soil column.

Facing the scarcity of measured data, it is difficult to check whether the calibration obtained by the semi-automated procedure is robust for outputs other than temperature. Possibilities exist to validate the calibration with electrical resistivity data (related to water/ice content) or direct soil moisture data but a thorough analysis of the quality of the present calibration or a calibration improvement by including these data in the calibration routine would be beyond the scope of this paper, especially as data do not exist for all sites. First tests have been made in this direction at STO, with promising results of a joint calibration using temperature and electrical resistivity data (Python, 2015). Efforts are also currently being made towards the installation of a soil moisture network in mountain environments (SNF project SOMOMOUNT, http://p3.snf.ch/project-143325). Soil moisture and geophysical monitoring data could then serve as additional validation of the thermal calibration (Pellet et al., 2016) as shown for the example of SCH (Fig. 9). Figure 9a and b show the soil moisture output of the model set-up giving the best fit with observed temperatures in comparison with on-site measured data that stem from soil moisture sensors adjacent to the borehole (see Hilbich et al., 2011). Although some biases are present, like the absolute value of the maximal peak in early summer (about 10 % mismatch at 12 cm), the absolute minimum during winter (about 7 % mismatch at 12 cm), or the stable summer maximum at 60 cm, the general behaviour is well reproduced: the mean values and the timing of freezing–thawing is satisfying. In a second step, we manually calibrated the soil physical parameter used in the water retention curve to define the minimal residual water, which also has a notable influence on the freezing-point depression. By this, the agreement with measured soil moisture was substantially improved (Fig. 9c and d), showing that model calibration can easily be improved if additional data sets are available. Figure 10 shows the resulting temperature difference at 10 m depth in the long-term simulations between the improved calibration and the reference run, indicating colder temperatures (~ 0.3 K) and later permafrost degradation at 10 m depth compared to the reference run.

7.3 RCM-based simulations

Given the various sources of uncertainty mentioned above and the choice of only one emission scenario (A1B) in the climate simulations, the results of the long-term simulation should not be considered as a prediction but rather as a projection of the range of the possible evolution of permafrost in the Swiss Alps under a given emission scenario. Our long-term simulations showed that the permafrost evolution is strongly influenced by the specific regional climate scenario applied (i.e. the specific GCM/RCM chain) but also by differently calibrated CoupModel set-ups. Climate scenario uncertainty appears to be the dominant component of uncertainty in this study.

A similar climate impact study has been carried out by Scherler et al. (2013), but with a different calibration procedure of the CoupModel and a different RCM downscaling technique for SCH and COR. In comparison to their results for SCH, the timing of permafrost degradation at 10 m around 2020–2030 and the moment when the entire seasonal thaw layer cannot refreeze anymore in winter are modelled similarly, but the consecutive warming after the start of degradation is smaller in the present study. Similarly, the 20 m layer shows a rapid degradation in Scherler et al. (2013), whereas it remains below the freezing point for most of the GCM/RCM chains in the present study. The discrepancies are mainly explained by a slightly different soil structure, which was part of the calibration approach in the present study. At COR, the results of Scherler et al. (2013) show slow warming at 10 and 20 m. In the present study, the warming is also slow, but once the 10 m layer is thawed, the warming propagates faster to deeper layers than in the results of Scherler et al. (2013); see Fig. 11. This difference is not surprising as Scherler et al. (2013) manually introduced a site-specific seasonal heat sink/source to compensate for the effect of air convection in the coarse blocky surface layer. By this, permafrost was conserved longer in the model than in a model set-up without parameterized convection. In ad-

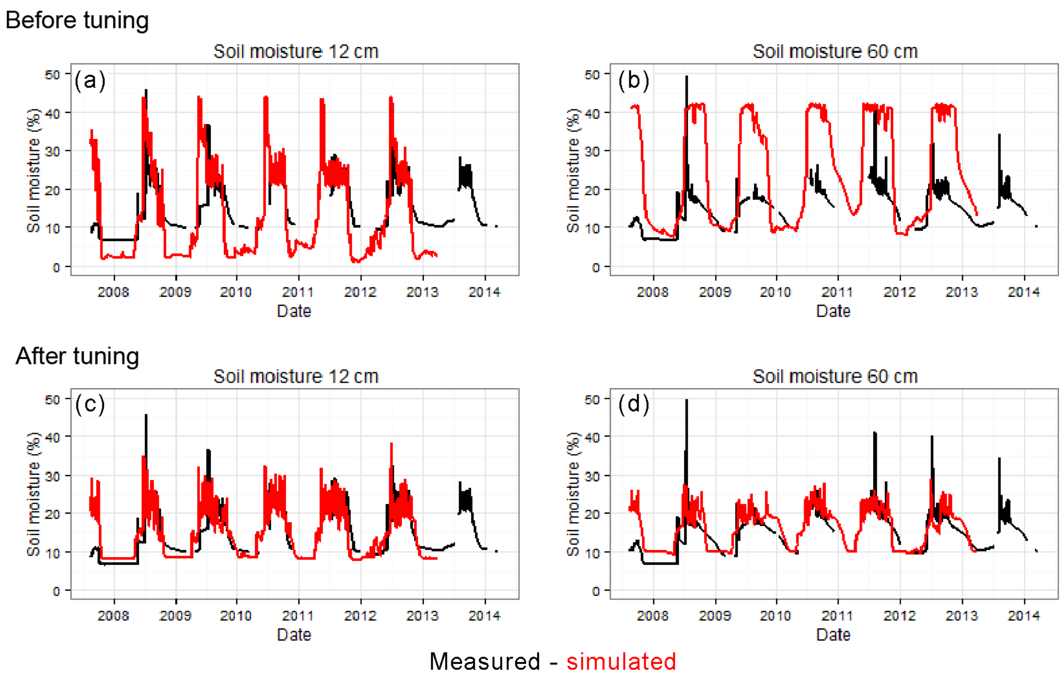

Figure 9. Comparison of the simulated (red) and measured (black) soil moisture data at 12 cm (left panels) and 60 cm (right panels) at SCH. Panels **(a)** and **(b)** show the results for soil moisture of the best thermal calibration, while **(c)** and **(d)** show the results after a further calibration of the soil physical parameter of the water retention curve, showing that the calibration can be further improved with additional data sets.

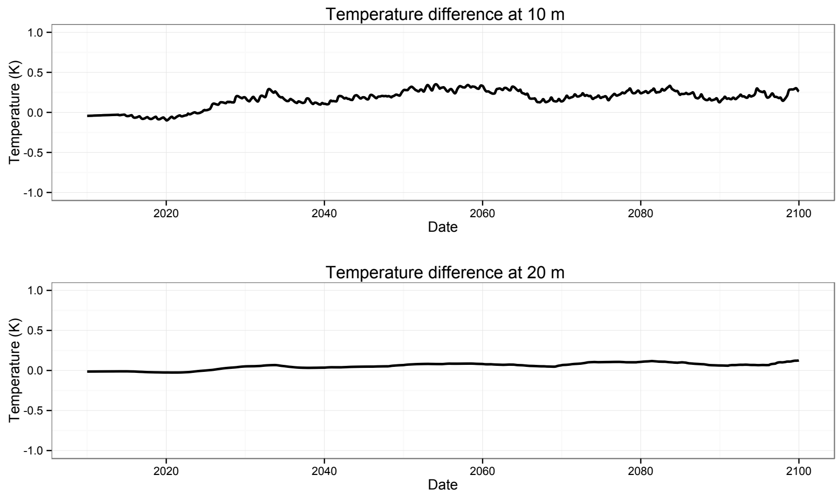

Figure 10. Difference in simulated 10 m temperature for the long-term simulation between the reference run for SCH (Fig. 7) and the improved calibration of Fig. 9c and d.

dition, higher ice contents within the rock glacier ice core were simulated in Scherler et al. (2013) than in the present study (85 % vs. 62 %, cf. Fig. 3), which decelerates warming as well. In contrast, the calibrated porosity values near the surface are higher in the present study (49 %) than the manually calibrated values of the previous study (10 %). Porosity values in heterogeneous rock glaciers are of course always highly uncertain, but it has to be noted that the best results of the GLUE procedure were not obtained with the highest porosities for the deeper layers: during the selection process, the consideration of the r^2 tended towards high porosities, but the best performances were obtained with lower porosities when considering the ME (cf. Fig. 3).

In contrast to Scherler et al. (2013), the cooling effect of convection in the coarse blocky surface layer was not hard-coded by an explicit source/sink term, but rather repre-

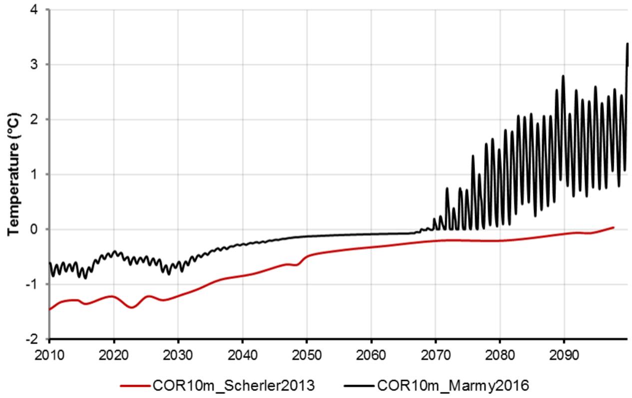

Figure 11. Comparison of the long-term simulation results for rock glacier Murtèl-Corvatsch at 10 m depth for the present study and the results obtained by Scherler et al. (2013) with the same model, but with a different calibration (see text for details).

sented indirectly through automatic adaption of site-specific subsurface parameters during calibration, e.g. a comparatively high albedo (∼ 25 %), low critical snow depth parameter and particularly a larger porosity (see above). Nevertheless, the absence of an explicit convection parameterization for coarse blocky subsurfaces is still the major shortcoming of the CoupModel regarding mountain permafrost applications (cf. also Staub et al., 2015), and it leads to a probable overestimation of the warming at this site (Fig. 11). However, it is not yet clear how the cooling by convection would evolve in a context of climate change and permafrost degradation, which is why an explicit treatment of this process would be favourable compared to the static, hard-coded energy source/sink approach used in Scherler et al. (2013).

At all six sites, significant permafrost degradation is projected, driven mostly by the projected increase in air temperature during snow-free periods and the prolongation of these periods due to snow cover decrease. This is in good agreement with earlier sensitivity studies using the same model (Marmy et al., 2013) and similar studies from other regions (Etzelmüller et al., 2011; Hipp et al., 2012). In general, the sites with blocky material and higher porosity (COR, LAP, MBP) show a lower sensitivity to climate change, whereas the bedrock sites (SCH and STO) tend to have a more rapid degradation. At most places, a high porosity is coupled with higher interstitial ice contents, hence requiring more energy to melt the ice and warm the ground.

Changes simulated in the snow cover duration are mostly influenced by the increasing air temperature and much less by the change in mean annual precipitation sum. This is in agreement with both Wang et al. (2014), who stated that the increase in atmospheric freezing level is responsible for most cryospheric changes in the future, and Steger et al. (2013), who found that Alpine snow cover changes in the ENSEMBLES GCM/RCM chains are mostly driven by temperature increases. Our CoupModel simulations showed a decrease of snow cover duration of about −20 to −37 %, which is on the same order of magnitude as the results by Bavay et al. (2009), who projected a mean reduction of snow cover duration of ∼ 30–35 % for two Alpine catchments (run under the B2 and A2 scenarios), and by Schmucki et al. (2014), who projected a decrease of snow cover of 32–35 % for high-elevation sites. These numbers are furthermore consistent with Steger et al. (2013), who analysed Alpine snow cover changes in the ENSEMBLES climate models themselves. During the next 10–20 years, this reduction of snow cover may have an opposite effect to ground warming in summer: a decrease of the snow cover in autumn and early winter can lead to a cooling of the ground because the cool winter temperature can better penetrate the ground with no snow cover or reduced snow cover. However, sensitivity studies for a whole range of air temperature and precipitation changes suggest that until the end of the century, the effect of warming will dominate over the potential cooling effect in late autumn/early winter (Marmy et al., 2013). In spring and late summer, the decrease of snow cover has always had a warming feedback because the snow is no longer present to isolate the ground from the positive summer temperatures.

The results of the long-term simulations have to be considered with caution as uncertainty may arise at several steps of the model chains: errors in the measurements used for calibration, structural errors of the model, choice of parameters and choice of their tested ranges, biases introduced during the calibration, emission scenario uncertainty or GCM/RCM chains' uncertainty.

8 Conclusion

The present paper tested a semi-automated method for a soil/permafrost model calibration, in order to be able to use it for a potentially large number of sites (e.g. in a distributed model). Other goals were to analyse the sensitivity of the model results to certain parameters, to identify site-specific processes that play a major role in the thermal regime at the individual permafrost sites and to use the calibrated model set-ups for long-term RCM-based simulations of the permafrost evolution.

The following conclusions can be drawn from the study.

- The method of semi-automated calibration using the Generalized Likelihood Uncertainty Estimation (GLUE) showed an efficient ability to reproduce permafrost conditions at several permafrost sites in the Swiss Alps: the upper boundary conditions were simulated precisely, whereas the absolute errors in the deepest layers were within a satisfactory error range. The r^2 at the surface ranged from 0.72 to 0.84, and the mean error at depth was usually smaller than 0.5 K, except at STO and RIT.

- Some site-specific characteristics, such as vertical or 2-D circulation of air (convection) or lateral flows of air and water, could not be reproduced by the approach, hence leading to warm biases at depth.
- The calibration of upper boundary parameters, especially parameters related to snow cover, was shown to have a large influence on the calibration performance, also in deeper ground layers. Therefore, efforts to obtain a precise upper boundary calibration must be undertaken, especially by increasing the length and the quality of surface measurements (ground surface temperature, radiation, snow cover, soil moisture etc.).
- The long-term simulations have shown a degradation trend at all sites, with an increasing active layer depth to at least 10 m at all sites until the end of the century, and even to 20 m at SCH and STO. However, strong uncertainty exists among the different GCMs/RCMs.
- The degradation is primarily driven by the change in air temperature during the snow-free period and the change in snow cover duration.
- The snow cover duration is projected to decrease by values between 20 and 37 %, and this decrease is mainly driven by the change in air temperature.
- In general, the calibration method can be suitable for large-scale or long-term modelling, but it is not recommended for site-specific process analysis if there are existing dominant processes that are not included in the CoupModel formulation. In these cases, manual calibration and parameterization of the missing processes have to be added. In comparison to other, simpler approaches to simulate future scenarios for borehole temperatures (as e.g. in Etzelmüller et al., 2011; Hipp et al., 2012 or, regarding spatial modelling, in Jafarov et al., 2012) the approach of this study focuses more on the understanding of the site-specific processes, while the long-term simulation results will not necessarily be better than results from simpler approaches as in the above cited studies. However, we believe that the considerably higher efforts of our approach are well justified by the knowledge gained regarding the effect of the dominant processes at the different sites. Of course, future work has to be directed into including the missing processes that have already been identified in the model formulation (i.e. convection).

We believe that the method presented here can be used as a starting point for large-scale modelling of the permafrost distribution in the Alps, provided that an increased number of sites with high-quality data series of observed ground temperature become available. A distributed model could be derived from the numerous calibrated sites by interpolation, in combination with digital elevation models, remote sensing data, ground surface temperature measurements and subsurface data from geophysical surveys.

9 Data availability

The borehole temperature data set of the PERMOS network is published under doi:10.13093/permos-2016-01 (for meta-data and borehole temperatures). The data are available at doi:10.13093/permos-2016-01. The downscaled GCM/RCM input data sets and the full set of COUP model simulation files including meta-data and parameter tables are stored at the Department of Geosciences and can be obtained through the corresponding author.

Appendix A: Nomenclature

Q_p	thermal quality of precipitation (fraction of solid) (–)
T_a	air temperature (°C)
F_liqmax	maximal liquid water content fraction in precipitation (default = 0.5) (–)
ρ_snow	density of snow ($\mathrm{kg\,m^{-3}}$)
k_snow	thermal conductivity of snow ($\mathrm{W\,m^{-1}\,°C^{-1}}$)
M_R	melting of snow due to solar radiation ($\mathrm{kg\,J^{-1}}$)
s_1, s_2	empirical parameters (–)
m_f	coefficient to take the refreezing into account
Δz_snow	snow depth (m)
M	total snowmelt ($\mathrm{mm\,day^{-1}}$)
R_{is}	global radiation ($\mathrm{MJ\,day^{-1}}$)
F_{q_h}	scaling coefficient (–)
L_f	latent heat of freezing ($\mathrm{J\,kg^{-1}}$)
F_bare	fraction of bare soil
R_snet	is the shortwave radiation ($\mathrm{W\,m^{-2}}$)
α	albedo (–)
ρ_a	density of air ($\mathrm{kg\,m^{-3}}$)
c_p	heat capacity of air ($1.004\,\mathrm{J\,g^{-1}\,K^{-1}}$)
γ	psychrometer constant ($66\,\mathrm{Pa\,K^{-1}}$)
r_as	aerodynamic resistance ($\mathrm{s\,m^{-1}}$)
e_surf	vapour pressure at the soil surface (mm water)
e_a	vapour pressure in air (mm water)
e_s	vapour pressure at saturation (mm water)
T_s	soil surface temperature (°C)
Ψ_1	water tension in the uppermost layer ($\mathrm{N\,m^{-1}}$)
M_water	molar mass of water ($18.016\,\mathrm{g\,mol^{-1}}$)
g	gravity constant ($9.81\,\mathrm{m\,s_{-2}}$)
R	gas constant ($8.31\,\mathrm{J\,K^{-1}\,mol^{-1}}$)
T_abszero	$-273.15\,°\mathrm{C}$
δ_surf	mass balance of water calculated at the surface (mm water)
k_tot	total unsaturated hydraulic conductivity ($\mathrm{mm\,day^{-1}}$)
k_w	saturated hydraulic conductivity ($\mathrm{mm\,day^{-1}}$)
S_e	effective saturation (%)
n and λ	empirical parameters (–)
a, g_n and g_m	empirical parameters (–)
Ψ	water tension ($\mathrm{N\,m^{-1}}$)
θ	water content (%)
θ_r	residual water content (%)
θ_y	threshold parameter for water tension (%)
k_unfrozen	thermal conductivity of unfrozen mineral soil ($\mathrm{W\,m^{-1}\,°C^{-1}}$)
h_1, h_2	empirical constants (–)
k_frozen	thermal conductivity of frozen mineral soils ($\mathrm{W\,m^{-1}\,°C^{-1}}$)
b_1, b_2, b_3, b_4	empirical parameters (–)
ρ_s	dry bulk soil density ($\mathrm{kg\,m^{-3}}$)

The Supplement related to this article is available online at doi:10.5194/tc-10-2693-2016-supplement.

Acknowledgements. We would like to acknowledge the Swiss National Science Foundation for the funding of the TEMPS project (project no. CRSII2 136279) as well as the Swiss PERMOS network for the data provided. A special thank you is given to Per-Erik Jansson from Kungliga Tekniska Högskolan of Stockholm for the technical and scientific support with the CoupModel. The critical and constructive comments of two reviewers very much helped to improve the manuscript.

Edited by: K. Isaksen
Reviewed by: two anonymous referees

References

Anisimov, O. A.: Potential feedback of thawing permafrost to the global climate system through methane emission, Environ. Res. Lett., 2, 045016, doi:10.1088/1748-9326/2/4/045016, 2007.

Anthony, K. M. W., Anthony, P., Grosse, G., and Chanton, J.: Geologic methane seeps along boundaries of Arctic permafrost thaw and melting glaciers, Nat. Geosci., 5, 419–426, 2012.

Arenson, L. U., Hoelzle, M., and Springman, S.: Borehole deformation measurements and internal structure of some rock glaciers in Switzerland, Permafrost Periglac., 13, 117–135, 2002.

Arenson, L. U., Hauck, C., Hilbich, C., Seward, L., Yamamoto, Y., and Springman, S. M.: Sub-surface heterogeneities in the Murtèl-Corvatsch rock glacier, Switzerland, in: Proceedings of the Sixth Canadian Permafrost Conference, Calgary, Alta, 12–16, 2010.

Atchley, A. L., Coon, E. T., Painter, S. L., Harp, D. R., and Wilson, C. J.: Influences and interactions of inundation, peat, and snow on active layer thickness, Geophys. Res. Lett., 43, 5116–5123, doi:10.1002/2016GL068550, 2016.

Barboux, C., Delaloye, R., Lambiel, C., Strozzi, T., Collet, C., and Raetzo, H: Surveying the activity of permafrost landforms in the Valais Alps with InSAR, in: Mattertal – ein Tal in Bewegung, edited by: Graf, C., Publikation zur Jahrestagung der Schweizerischen Geomorphologischen Gesellschaft, 29, 7–19, 2013.

Bavay, M., Lehning, M., Jonas, T., and Löwe, H.: Simulations of future snow cover and discharge in Alpine headwater catchments, Hydrol. Process., 23, 95–108, 2009.

Begert, M., Seiz, G., Schlegel, T., Musa, M., Baudraz, G., and Moesch, M.: Homogenisierung von Klimamessreihen der Schweiz und Bestimmung der Normwerte 1961–1990, Schlussbericht des Projekts NORM90, MeteoSchweiz, Zürich, 2003.

Beven, K.: Towards a coherent philosophy for modelling the environment, P. Roy. Soc. Lond. A, 458, 2465–2484, 2002.

Beven, K. and Binley, A.: The future of distributed models: model calibration and uncertainty prediction, Hydrol. Process., 6, 279–298, 1992.

Beven, K. and Freer, J.: Equifinality, data assimilation, and uncertainty estimation in mechanistic modelling of complex environmental systems using the GLUE methodology, J. Hydrol., 249, 11–29, 2001.

Boeckli, L., Brenning, A., Gruber, S., and Noetzli, J.: A statistical approach to modelling permafrost distribution in the European Alps or similar mountain ranges, The Cryosphere, 6, 125–140, doi:10.5194/tc-6-125-2012, 2012.

Bommer, C., Phillips, M., and Arenson, L. U.: Practical recommendations for planning, constructing and maintaining infrastructure in mountain permafrost, Permafrost Periglac., 21, 97–104, 2010.

Bosshard, T., Kotlarski, S., Zappa, M., and Schär, C.: Hydrological Climate-Impact Projections for the Rhine River: GCM–RCM Uncertainty and Separate Temperature and Precipitation Effects, J. Hydrometeorol., 15, 697–713, 2014.

Chadburn, S., Burke, E., Essery, R., Boike, J., Langer, M., Heikenfeld, M., Cox, P., and Friedlingstein, P.: An improved representation of physical permafrost dynamics in the JULES land–surface model, Geosci. Model Dev., 8, 1493–1508, doi:10.5194/gmd-8-1493-2015, 2015.

Cremonese, E., Gruber, S., Phillips, M., Pogliotti, P., Boeckli, L., Noetzli, J., Suter, C., Bodin, X., Crepaz, A., Kellerer-Pirklbauer, A., Lang, K., Letey, S., Mair, V., Morra di Cella, U., Ravanel, L., Scapozza, C., Seppi, R., and Zischg, A.: Brief Communication: "An inventory of permafrost evidence for the European Alps", The Cryosphere, 5, 651–657, doi:10.5194/tc-5-651-2011, 2011.

Cui, T., Fox, C., and O'Sullivan, M. J.: Bayesian calibration of a large-scale geothermal reservoir model by a new adaptive delayed acceptance Metropolis Hastings algorithm, Water Resour. Res., 47, W10521, doi:10.1029/2010WR010352, 2011.

Delaloye, R.: Contribution à l'étude du pergélisol de montagne en zone marginale, Doctoral dissertation, Université de Fribourg, Fribourg, 2004.

Delaloye, R. and Lambiel, C.: Evidence of winter ascending air circulation throughout talus slopes and rock glaciers situated in the lower belt of alpine discontinuous permafrost (Swiss Alps), Norweg. J. Geogr., 59, 194–203, 2005.

Ekici, A., Beer, C., Hagemann, S., Boike, J., Langer, M., and Hauck, C.: Simulating high-latitude permafrost regions by the JSBACH terrestrial ecosystem model, Geosci. Model Dev., 7, 631–647, doi:10.5194/gmd-7-631-2014, 2014.

Ekici, A., Chadburn, S., Chaudhary, N., Hajdu, L. H., Marmy, A., Peng, S., Boike, J., Burke, E., Friend, A. D., Hauck, C., Krinner, G., Langer, M., Miller, P. A., and Beer, C.: Site-level model intercomparison of high latitude and high altitude soil thermal dynamics in tundra and barren landscapes, The Cryosphere, 9, 1343–1361, doi:10.5194/tc-9-1343-2015, 2015.

Endrizzi, S., Gruber, S., Dall'Amico, M., and Rigon, R.: GEOtop 2.0: simulating the combined energy and water balance at and below the land surface accounting for soil freezing, snow cover and terrain effects, Geosci. Model Dev., 7, 2831–2857, doi:10.5194/gmd-7-2831-2014, 2014.

Engelhardt, M., Hauck, C., and Salzmann, N.: Influence of atmospheric forcing parameters on modelled mountain permafrost evolution, Meteorol. Z., 19, 491–500, 2010.

Etzelmüller, B., Heggem, E. S., Sharkhuu, N., Frauenfelder, R., Kääb, A., and Goulden, C: Mountain permafrost distribution modelling using a multi-criteria approach in the Hövsgöl area, northern Mongolia, Permafrost Periglac., 17, 91–104, 2006.

Etzelmüller, B., Schuler, T. V., Isaksen, K., Christiansen, H. H., Farbrot, H., and Benestad, R.: Modeling the temperature evolution of Svalbard permafrost during the 20th and 21st century, The Cryosphere, 5, 67–79, doi:10.5194/tc-5-67-2011, 2011.

Fiddes, J., Endrizzi, S., and Gruber, S.: Large-area land surface simulations in heterogeneous terrain driven by global data sets: application to mountain permafrost, The Cryosphere, 9, 411–426, doi:10.5194/tc-9-411-2015, 2015.

Finsterle, S., Sonnenthal, E. L., and Spycher, N.: Advances in subsurface modeling using the TOUGH suite of simulators, Comput. Geosci., 65, 2–12, 2012.

Gärtner-Roer, I.: Sediment transfer rates of two active rockglaciers in the Swiss Alps, Geomorphology, 167–168, 45–50, 2012.

Gisnås, K., Westermann, S., Schuler, T. V., Melvold, K., and Etzelmüller, B.: Small-scale variation of snow in a regional permafrost model, The Cryosphere, 10, 1201–1215, doi:10.5194/tc-10-1201-2016, 2016.

Gruber, S. and Hoelzle, M.: Statistical modelling of mountain permafrost distribution: local calibration and incorporation of remotely sensed data, Permafrost Periglac., 12, 69–77, 2001.

Gruber, S., King, L., Kohl, T., Herz, T., Haeberli, W., and Hoelzle, M.: Interpretation of geothermal profiles perturbed by topography: The Alpine permafrost boreholes at Stockhorn Plateau, Switzerland, Permafrost Periglac., 15, 349–357, 2004.

Gubler, S., Endrizzi, S., Gruber, S., and Purves, R. S.: Sensitivities and uncertainties of modeled ground temperatures in mountain environments, Geosci. Model Dev., 6, 1319–1336, doi:10.5194/gmd-6-1319-2013, 2013.

Haeberli, W.: Pilot analysis of permafrost cores from the active rock glacier Murtèl I, Piz Corvatsch, Eastern Swiss Alps, Versuchsanstalt für Wasserbau, Hydrologie und Glaziologie, ETH Zürich, 1990.

Haeberli, W., Hoelzle, M., Kääb, A., Keller, F., Vonder Mühll, D., and Wagner, S.: Ten years after drilling through the permafrost of the active rock glacier Murtèl, Eastern Swiss Alps: answered questions and new perspectives, in: Proceedings 7th International Conference on Permafrost, Centre d'Etudes Nordiques, Université Laval, Yellowknife, Canada, 1998.

Harris, C., Mühll, D. V., Isaksen, K., Haeberli, W., Sollid, J. L., King, L., Holmlund, P., Dramis, F., Guglielmin, M., and Palacios, D.: Warming permafrost in European mountains, Global Planet. Change, 39, 215–225, 2003.

Harris, C., Arenson, L. U., Christiansen, H. H., Etzelmüller, B., Frauenfelder, R., Gruber, S., Haeberli, W., Hauck, C., Hölzle, M., Humlum, O., Isaksen, K., Kääb, A., Kern-Lütschg, M., Lehning, M., Matsuoka, N., Murton, J. B., Nötzli, J., Phillips, M., Ross, N., Seppälä, M., Springman, S. M., and Vonder Mühll, D.: Permafrost and climate in Europe: Monitoring and modelling thermal, geomorphological and geotechnical responses, Earth-Sci. Rev., 92, 117–171, 2009.

Hartikainen, J., Kouhia, R., and Wallroth, T.: Permafrost simulations at Forsmark using a numerical 2D thermo-hydro-chemical model, Svensk Kärnbränslehantering AB, Swedish Nuclear Fuel and Waste Management Company, Stockholm, 2010.

Hauck, C.: Frozen ground monitoring using DC resistivity tomography, Geophys. Res. Lett., 29, 12-1–12-4, 2002.

Hauck, C., Delaloye, R., Roer, I. H., Hilbich, C., Hoelzle, M., Kenner, R., Kotlarski, S., Lambiel, C., Marmy, A., Müller, J., Noetzli, J., Phillips, M., Rajczak, J., Salzmann, N., Schaepman, M. E., Schär, C., Staub, B., and Völksch, I.: The Evolution of Mountain Permafrost in Switzerland, in: AGU Fall Meeting Abstracts, 1, 04, 2013.

Heerema, K., Booij, M. J., Huting, R., Warmink, J. J., van Beek, E., and Jigjsuren, O.: Modelling impacts of climate change on the hydrology of a Mongolian catchment using an appropriate permafrost conceptualization, in: EGU General Assembly Conference Abstracts, 15, 4525, 2013.

Herz, T., King, L., and Gubler, H.: Thermal regime of coarse debris layers in the Ritigraben catchment, Matter valley, Swiss Alps, in: Eighth International Conference on Permafrost, Zürich, 2003.

Hilbich, C.: Geophysical monitoring systems to assess and quantify ground ice evolution in mountain permafrost, Doctoral dissertation, Univ., Diss., Jena, 2009.

Hilbich, C.: Time-lapse refraction seismic tomography for the detection of ground ice degradation, The Cryosphere, 4, 243–259, doi:10.5194/tc-4-243-2010, 2010.

Hilbich, C., Hauck, C., Hoelzle, M., Scherler, M., Schudel, L., Völksch, I., Vonder Mühll, D., and Mäusbacher, R.: Monitoring mountain permafrost evolution using electrical resistivity tomography: A 7-year study of seasonal, annual, and long-term variations at Schilthorn, Swiss Alps, J. Geophys. Res., 113, F01S90, doi:10.1029/2007JF000799, 2008.

Hilbich, C., Marescot, L., Hauck, C., Loke, M. H., and Mäusbacher, R.: Applicability of Electrical Resistivity Tomography Monitoring to Coarse Blocky and Ice-rich Permafrost Landforms, Permafrost Periglac., 20, 269–284, 2009.

Hilbich, C., Fuss, C., and Hauck, C.: Automated Time-lapse ERT for Improved Process Analysis and Monitoring of Frozen Ground, Permafrost Periglac., 22, 306–319, 2011.

Hipp, T., Etzelmüller, B., Farbrot, H., Schuler, T. V., and Westermann, S.: Modelling borehole temperatures in Southern Norway – insights into permafrost dynamics during the 20th and 21st century, The Cryosphere, 6, 553–571, doi:10.5194/tc-6-553-2012, 2012.

Hoelzle, M. and Gruber, S.: Borehole and ground surface temperatures and their relationship to meteorological conditions in the Swiss Alps, in: Proceedings Ninth International Conference on Permafrost, Fairbanks, 723–728, 2008.

Hoelzle, M., Mittaz, C., Etzelmüller, B., and Haeberli, W.: Surface energy fluxes and distribution models of permafrost in European mountain areas: an overview of current developments, Permafrost Periglac., 12, 53–68, 2001.

Hoelzle, M., Mühll, D. V., and Haeberli, W.: Thirty years of permafrost research in the Corvatsch-Furtschellas area, Eastern Swiss Alps: A review, Norweg. J. Geogr., 56, 137–145, 2002.

Jafarov, E. E., Marchenko, S. S., and Romanovsky, V. E.: Numerical modeling of permafrost dynamics in Alaska using a high spatial resolution dataset, The Cryosphere, 6, 613–624, doi:10.5194/tc-6-613-2012, 2012.

Jansson, P.-E.: CoupModel: Model use, calibration and validation, T. ASABE, 55, 1335–1344, 2012.

Jansson, P.-E. and Karlberg, L.: Coupled heat and mass transfer model for soil-plant-atmosphere systems, Royal Institute of Technology, Dept. of Civil and Environmental Engineering, Stockholm, 2004.

Kääb, A. and Kneisel, C.: Permafrost creep within a recently deglaciated glacier forefield: Muragl, Swiss Alps, Permafrost Periglac., 17, 79–85, 2006.

Kääb, A., Frauenfelder, R., and Roer, I.: On the response of rockglacier creep to surface temperature increase, Global Planet. Change, 56, 172–187, 2007.

Kotlarski, S., Keuler, K., Christensen, O. B., Colette, A., Déqué, M., Gobiet, A., Goergen, K., Jacob, D., Lüthi, D., van Meijgaard, E., Nikulin, G., Schär, C., Teichmann, C., Vautard, R., Warrach-Sagi, K., and Wulfmeyer, V.: Regional climate modeling on European scales: a joint standard evaluation of the EURO-CORDEX RCM ensemble, Geosci. Model Dev., 7, 1297–1333, doi:10.5194/gmd-7-1297-2014, 2014.

Kendon, E. J., Jones, R. G., Kjellström, E., and Murphy, J. M.: Using and designing GCM-RCM ensemble regional climate projections, J. Climate, 23, 6485–6503, 2010.

King, L.: Soil and rock temperatures in discontinuous permafrost: Gornergrat and Unterrothorn, Wallis, Swiss Alps, Permafrost Periglac., 1, 177–188, 1990.

Lambiel, C.: Le pergélisol dans les terrains sédimentaires à forte déclivité: distribution, régime thermique et instabilités, PhD thesis, Institut de Géographie, coll. "Travaux et Recherches" no. 33, Université de Lausanne, Lausanne, p. 260, 2006.

Langer, M., Westermann, S., Heikenfeld, M., Dorn, W., and Boike, J.: Satellite-based modeling of permafrost temperatures in a tundra lowland landscape, Remote Sens. Environ., 135, 12–24, 2013.

Lehning, M., Löwe, H., Ryser, M., and Raderschall, N.: Inhomogeneous precipitation distribution and snow transport in steep terrain, Water Resour. Res., 44, W07404, doi:10.1029/2007WR006545, 2008.

Lepage, J. M. and Doré, G.: Experimentation of mitigation techniques to reduce the effects of permafrost degradation on transportation infrastructures at Beaver Creek experimental road site, in: Proc. 63rd Canadian Geotechnical Conference, Calgary, Alberta, 2010.

Lindeman, R. H., Merenda, P. F., and Gold, R. Z.: Introduction to bivariate and multivariate analysis, Scott, Foresman, Glenview, IL, 1980.

Luethi, R., Phillips, M., and Lehning, M.: Estimating Non-Conductive Heat Flow Leading to Intra-Permafrost Talik Formation at the Ritigraben Rock Glacier (Western Swiss Alps), Permafrost Periglac., doi:10.1002/ppp.1911, 2016.

Luetschg, M., Lehning, M., and Haeberli, W.: A sensitivity study of factors influencing warm/thin permafrost in the Swiss Alps, J. Glaciol., 54, 696–704, 2008.

Marmy, A., Salzmann, N., Scherler, M., and Hauck, C.: Permafrost model sensitivity to seasonal climatic changes and extreme events in mountainous regions, Environ. Res. Lett., 8, 035048, doi:10.1088/1748-9326/8/3/035048, 2013.

McColl, S. T.: Paraglacial rock-slope stability, Geomorphology, 153, 1–16, 2012.

Mittaz, C., Hoelzle, M., and Haeberli, W.: First results and interpretation of energy-flux measurements over Alpine permafrost, Ann. Glaciol., 31, 275–280, 2000.

Morton, A.: Mathematical models: questions of trustworthiness, Brit. J. Philos. Sci., 44, 659–674, 1993.

Mott, R., Schirmer, M., Bavay, M., Grünewald, T., and Lehning, M.: Understanding snow-transport processes shaping the mountain snow-cover, The Cryosphere, 4, 545–559, doi:10.5194/tc-4-545-2010, 2010.

Mountain Research Initiative EDW Working Group: Elevation-dependent warming in mountain regions of the world, Nat. Clim. Change, 5, 424–430, 2015.

Nakicenovic, N. and Swart, R.: IPCC – Special Report on Emission Scenarios, Summary for Policy Makers, Cambridge University Press, Cambridge, 2000.

Noetzli, J. and Gruber, S.: Transient thermal effects in Alpine permafrost, The Cryosphere, 3, 85–99, doi:10.5194/tc-3-85-2009, 2009.

Noetzli, J., Gruber, S., Kohl, T., Salzmann, N., and Haeberli, W.: Three-dimensional distribution and evolution of permafrost temperatures in idealized high-mountain topography, J. Geophys. Res., 112, F02S13, doi:10.1029/2006JF000545, 2007.

Noetzli, J., Hilbich, C., Hauck, C., Hoelzle, M., and Gruber, S.: Comparison of simulated 2D temperature profiles with time-lapse electrical resistivity data at the Schilthorn crest, Switzerland, in: Ninth International Conference on Permafrost, Vol. 29, University of Alaska, Fairbanks, 1293–1298, 2008.

Pellet, C., Hilbich, C., Marmy, A., and Hauck, C.: Soil Moisture Data for the Validation of Permafrost Models Using Direct and Indirect Measurement Approaches at Three Alpine Sites, Front. Earth Sci., 3, 91, doi:10.3389/feart.2015.00091, 2016.

PERMOS: Permafrost in Switzerland 2010/2011 to 2013/2014, edited by: Noetzli, J., Luethi, R., and Staub, B., Glaciological Report (Permafrost) No. 12-15 of the Cryospheric Commission of the Swiss Academy of Sciences, 85 pp., 2016.

PERMOS data: PERMOS Database, Swiss Permafrost Monitoring Network, Fribourg, Switzerland, doi:10.13093/permos-2016-01, 2016.

Phillips, M.: Avalanche defence strategies and monitoring of two sites in mountain permafrost terrain, Pontresina, Eastern Swiss Alps, Nat. Hazards, 39, 353–379, 2006.

Python, S.: Technical improvement of the 4-phase model to better assess the ice, wáter and air content estimation in permafrost substrates, Master thesis, Department of Geosciences, University of Fribourg, Fribourg, Switzerland, 2015.

Romanovsky, V. E., Smith, S. L., and Christiansen, H. H.: Permafrost thermal state in the polar Northern Hemisphere during the international polar year 2007–2009: a synthesis. Permafrost Periglac., 21, 106–116, doi:10.1002/ppp.689, 2010.

Quinton, W. L., Hayashi, M., and Chasmer, L. E.: Permafrost-thaw-induced land-cover change in the Canadian subarctic: implications for water resources, Hydrol. Process., 25, 152–158, 2011.

Rajczak, J., Kotlarski, S., Salzmann, N., and Schär, C.: Robust climate scenarios for sites with sparse observations: a two-step bias correction approach, Int. J. Climatol., 36, 1226–1243, 2016.

Rist, A., Phillips, M., and Haeberli, W.: Influence of snow meltwater infiltration on active layer movement in steep alpine scree slopes within the discontinuous mountain permafrost, in: Proceedings, Asian Conference on Permafrost, Lanzhou, 10–11, 2006.

Sattler, K., Anderson, B., Mackintosh, A., Norton, K., and de Róiste, M.: Estimating permafrost distribution in the maritime Southern Alps, New Zealand, based on climatic conditions at rock glacier sites, Front. Earth Sci., 4, 4, doi:10.3389/feart.2016.00004, 2016.

Scapozza, C., Baron, L., and Lambiel, C.: Borehole logging in Alpine periglacial talus slopes (Valais, Swiss Alps), Permafrost Periglac., 26, 67–83, 2015.

Schär, C., Vidale, P. L., Lüthi, D., Frei, C., Häberli, C., Liniger, M. A., and Appenzeller, C.: The role of increasing temperature variability in European summer heatwaves, Nature, 427, 332–336, 2004.

Scherler, M., Hauck, C., Hoelzle, M., Stähli, M., and Völksch, I.: Meltwater infiltration into the frozen active layer at an alpine permafrost site, Permafrost Periglac., 21, 325–334, 2010.

Scherler, M., Hauck, C., Hoelzle, M., and Salzmann, N.: Modeled sensitivity of two alpine permafrost sites to RCM-based climate scenarios, J. Geophys. Res.-Ea. Surf., 118, 780–794, 2013.

Scherler, M., Schneider, S., Hoelzle, M., and Hauck, C.: A two-sided approach to estimate heat transfer processes within the active layer of the Murtèl–Corvatsch rock glacier, Earth Surf. Dynam., 2, 141–154, doi:10.5194/esurf-2-141-2014, 2014.

Schmucki, E., Marty, C., Fierz, C., and Lehning, M.: Simulations of 21st century snow response to climate change in Switzerland from a set of RCMs, Int. J. Climatol., 35, 3262–3273, doi:10.1002/joc.4205, 2014.

Schneider, S., Hoelzle, M., and Hauck, C.: Influence of surface and subsurface heterogeneity on observed borehole temperatures at a mountain permafrost site in the Upper Engadine, Swiss Alps, The Cryosphere, 6, 517–531, doi:10.5194/tc-6-517-2012, 2012.

Schneider, S., Daengeli, S., Hauck, C., and Hoelzle, M.: A spatial and temporal analysis of different periglacial materials by using geoelectrical, seismic and borehole temperature data at Murtèl–Corvatsch, Upper Engadin, Swiss Alps. Geogr. Helv., 68, 265–280, 2013.

Staub, B., Marmy, A., Hauck, C., Hilbich, C., and Delaloye, R.: Ground temperature variations in a talus slope influenced by permafrost: a comparison of field observations and model simulations, Geogr. Helv., 70, 45–62, 2015.

Staub, B. and Delaloye, R.: Using near-surface ground temperature data to derive snow insulation and melt indices for mountain permafrost applications, Permafrost Periglac., doi:10.1002/ppp.1890, in press, 2016.

Steger, C., Kotlarski, S., Jonas, T., and Schär, C.: Alpine snow cover in a changing climate: a regional climate model perspective, Clim. Dynam., 41, 735–754, 2013.

Themessl, M. J., Gobiet, A., and Leuprecht, A.: Empirical-statistical downscaling and error correction of daily precipitation from regional climate models, Int. J. Climatol., 31, 1530–1544, doi:10.1002/joc.2168, 2011.

Tonkin, M. and Doherty, J.: Calibration-constrained Monte Carlo analysis of highly parameterized models using subspace techniques, Water Resour. Res., 45, W00B10, doi:10.1029/2007WR006678, 2009.

Torma, C., Giorgi, F., and Coppola, E.: Added value of regional climate modeling over areas characterized by complex terrain – Precipitation over the Alps, J. Geophys. Res.-Atmos., 120, 3957–3972, doi:10.1002/2014JD022781, 2015.

Trombotto, D.: Survey of cryogenic processes, periglacial forms and permafrost conditions in South America, Revista do Instituto Geológico, 21, 33–55, 2000.

Van der Linden, P. and Mitchell, J. E. (Eds.): ENSEMBLES: Climate Change and its Impacts: Summary of research and results from the ENSEMBLES project, Met Office Hadley Centre, Exeter, UK, 160 pp., 2009.

Vieira, G., Bockheim, J., Guglielmin, M., Balks, M., Abramov, A. A., Boelhouwers, J., Cannone, N., Ganzert, L., Gilichinsky, A. A., Goryachkin, S., Lopez-Martinez, J., Meiklejohn, I., Raffi, R., Ramo, M., Schaefer, C., Serrano, E., Simas, F., Sletten, R., and Wagner, D.: Thermal state of permafrost and active-layer monitoring in the Antarctic: Advances during the international polar year 2007–2009, Permafrost Periglac., 21, 182–197, 2010.

Vonder Mühll, D. and Haeberli, W.: Thermal characteristics of the permafrost within an active rock glacier (Murtèl/Corvatsch, Grisons, Swiss Alps), J. Glaciol., 36, 151–158, 1990.

Vonder Mühll, D. S., Hauck, C., and Lehmann, F.: Verification of geophysical models in Alpine permafrost using borehole information, Ann. Glaciol., 31, 300–306, 2000.

Vonder Mühll, D. S., Hauck, C., Gubler, H., McDonald, R., and Russill, N.: New geophysical methods of investigating the nature and distribution of mountain permafrost with special reference to radiometry techniques, Permafrost Periglac., 12, 27–38, 2001.

Wang, S., Zhang, M., Pepin, N. C., Li, Z., Sun, M., Huang, X., and Wang, Q.: Recent changes in freezing level heights in High Asia and their impact on glacier changes, J. Geophys. Res., 119, 1753–1765, 2014.

Weiming, C., Shangmin, Z., Chenghu, Z., and Xi, C.: Simulation of the Decadal Permafrost Distribution on the Qinghai-Tibet Plateau (China) over the Past 50 Years, Permafrost Periglac., 23, 292–300, 2012.

Westermann, S., Schuler, T. V., Gisnås, K., and Etzelmüller, B.: Transient thermal modeling of permafrost conditions in Southern Norway, The Cryosphere, 7, 719–739, doi:10.5194/tc-7-719-2013, 2013.

Westermann, S., Elberling, B., Højlund Pedersen, S., Stendel, M., Hansen, B. U., and Liston, G. E.: Future permafrost conditions along environmental gradients in Zackenberg, Greenland, The Cryosphere, 9, 719–735, doi:10.5194/tc-9-719-2015, 2015.

Westermann, S., Langer, M., Boike, J., Heikenfeld, M., Peter, M., Etzelmüller, B., and Krinner, G.: Simulating the thermal regime and thaw processes of ice-rich permafrost ground with the land–surface model CryoGrid 3, Geosci. Model Dev., 9, 523–546, doi:10.5194/gmd-9-523-2016, 2016.

Zenklusen Mutter, E. and Phillips, M.: Active layer characteristics at ten borehole sites in alpine permafrost terrain, Switzerland, Permafrost Periglac., 23, 138–151, 2012.

Zenklusen Mutter, E., Blanchet, J., and Phillips, M.: Analysis of ground temperature trends in Alpine permafrost using generalized least squares, J. Geophys. Res.-Ea. Surf., 115, F04009, doi:10.1029/2009JF001648, 2010.

Zhang, Y., Li, J., Wang, X., Chen, W., Sladen, W., Dyke, L., Dredge, L., Poitevin, J., McLennan, D., Stewart, H., Kowalchuk, S., Wu, W., Kershaw, P., and Brook, R. K.: Modelling and mapping permafrost at high spatial resolution in Wapusk National Park, Hudson Bay Lowlands, Can. J. Earth Sci., 49, 925–937, 2012.